April 9th 2010

To: Dr. Julio Militzer
Dr. Marek Kujath

From: Team 12
Loading Apparatus for High Velocity Tissue Rupture

Geoff Beck
Ben Breen
Rachael Schwartz
Ruth Domaratzki

Re: Winter Term Report

April 9, 2010

Team 12 designed an apparatus to perform uniaxial tensile tests on biological materials. The apparatus is capable of conducting tensile tests at rates of strain above those currently attainable at the Dalhousie Department of Biomedical Engineering. The design overcomes strain rate limitations inherent with the currently employed servo-hydraulically actuated model at the sacrifice of other features on the present device that are not required in the current research being conducted by the client. Such features include the ability to conduct biaxial tests. The enclosed document outlines our successes and shortfalls in the construction of this device.

Team 12 – Loading Apparatus for High Velocity Tissue Rupture

Geoff Beck _____
Ben Breen _____
Rachael Schwartz _____
Ruth Domaratzki _____

MECH 4020 – Design Project II

Team 12
Loading Apparatus for High Velocity Tissue Rupture

Geoff Beck
Ben Breen
Rachael Schwartz
Ruth Domaratzki

Supervisor
Dr. M. Kujath

Client
Dr. M. Lee

Abstract

In fulfillment of a Mechanical Engineering degree, Team 12 (2009-2010) completed the Design Project courses, MECH 4010 and MECH 4020, in the fall and winter semesters.

The team has created a loading apparatus for high velocity tissue rupture for the Department of Biomedical Engineering. The device held a design criterion of fracturing a specimen of bovine tendon (up to 2.5cm) at a strain rate of $1000s^{-1}$, recording force, position, and velocity (vs. time). This report describes the design, construction, and testing of this senior design project.

Our device when tested, was capable of reaching linear velocities of 7000 mm/s in the specimen track, which would correspond to a strain-rate of $800s^{-1}$ for a typical sample. The period of acceleration however covered a longer distance than was reasonable for the client, so some additional modifications would be necessary before publication-quality tests are capable from this device. All measurements were verified through the use of high-speed camera imagery.

Table of Contents

1 Introduction 1
1.1 Background 1
1.2 Tissue Mechanics 2
2 Objectives 4
3 Generation of Alternatives 6
3.1 Hopkinson Split Bar Apparatus 6
3.2 Gravitational Impact Pendulum 7
4 Selected Design 8
4.1 Design Evolution 8
4.2 Design Selection Matrices 10
5 Problem Exploration 10
5.1 Modeling 10
5.1.1 LAHVTR Mock-Up 10
5.1.2 Finite Element Analysis 11
5.1.3 Rapid Prototyping 11
5.2 Testing 12
5.2.1 Biological Specimen Testing 12
5.2.2 Solenoid Testing 12
6 Calculations 13
7 Final Design 16
7.1 Drive Shaft Assembly 16
7.1.1 Flywheel Design 17
7.1.2 Main Shaft 19
7.1.3 Gripping Mechanism 20
7.1.4 Damper 20
7.1.5 Safety Shield 21
7.2 Electrical Components 21
7.2.1 Motor and Frequency Drive 21
7.2.2 Measurement Systems 22
7.2.3 Solenoid Actuation 24
8 Implementation of Measurement Systems 26
8.1 Calibration of LVDT 26
8.2 Calibration of Force Transducer 26
9 Safety 27
10 Testing 27
10.1 Test Procedure 27
10.2 Validation Method 28
10.3 Measurement Equipment Testing Results 28
10.4 High Speed Video Testing Results 31
10.5 Time of Impact Analysis 34
11 Issues Encountered 35
11.1 Electrical and Mechanical Crosstalk 35

12 Impact on Society 35
13 Life Cycle Analysis 36
14 Work Allotment 36
15 Budget 36
16 Future Considerations 37
16.1 Control of Initial Sample Length 37
16.2 Prevent deformation of critical components 38
16.3 Other Considerations 39
17 Conclusions 39
18 References 40
19 Appendices 40
Appendix A– Previously Signed Documents 40
Appendix B: Decision-Making Tables and Charts 44
Appendix C: Gantt Chart 46
Appendix D: Budget 47
Appendix E: User's Manual 49
Appendix F: Engineering Drawings 55

List of Figures

Figure 1: Crosslinking of Collagen Fibers (Lee, 2010) 2
Figure 2: Strength and Stiffness Relationships for Materials (Lee, 2010) 2
Figure 3: Structural-Mechanical Relations in Soft Tissues (Lee, 2010) 3
Figure 4: Hopkinson Split Bar Apparatus 7
Figure 5: Gravitational Impact Pendulum 8
Figure 6: Early depiction of LAHVTR 9
Figure 7: Mock-up of Device 11
Figure 8: Rapid Prototype of Device 11
Figure 9: Solenoid voltage vs Time (theoretical-red, experimental-blue) 13
Figure 10: Desired vs Anticipated Strain Rate 13
Figure 11: Final Design 16
Figure 12: Drive shaft Assembly 17
Figure 13: Flywheel 18
Figure 14: Flywheel Design 18
Figure 15: Engagement Pin in Flywheel 19
Figure 16: Exploded View of Drive Shaft Assembly 19
Figure 17: Exploded Grip Assembly 20
Figure 18: Damper set-up 21
Figure 19 - Diagram of Safety Shield 21
Figure 20: Frequency Controller 22
Figure 21: Specimen Force Measurement 23
Figure 22: Wheatstone Bridge Configuration 24
Figure 23: Initial Position of Contact Tooth 25
Figure 24: Final Position of Contact Tooth 25

Figure 26: Calibration Graph for LVDT 26
Figure 27: Calibration Graph for Force Transducer 27
Figure 28: Raw Signals Acquired During Testing 29
Figure 29: Processed Signals 29
Figure 30: Velocity vs. Time Analysis 30
Figure 31: Documented Force vs. Displacement Characteristic for Sample 30
Figure 32: Force-Displacement Characteristic Obtained 31
Figure 33: Creating a reference system for high-speed video analysis. 32
Figure 34: High-speed video frames and feature tracking for 8mm sample at 500RPM and 500 frames per second. 32
Figure 35: Mechanical Cross-Coupling 35
Figure 36: Current control of sample length 38
Figure 37: Cross-sectional view of spring loaded tooth. 39

List of Tables

Table 1: Mechanical Properties of Collagen and Elastin (Lee, 2010) 3
Table 2: Content and Mechanical Properties of Soft Tissue Composites (Lee, 2010) 4
Table 3: Design Requirements Check list 4
Table 4: Biological Specimen Testing Results 12
Table 5: Displacement data for 500RPM trial with 8mm sample 32
Table 2: Displacement data for 1000RPM trial with 8mm sample 33
Table 5: Comparative Chart of Estimated to Actual Machining Hours 36
Table 6: Comparative Graph of Estimated to Actual Budget 36

1 Introduction

1.1 Background

The standard uniaxial tensile tension test reveals many fundamental properties of materials. Properties of the material such as the ultimate tensile stress, toughness, failure modes and failure location are often sought. The results of uniaxial tensile tests can be applied through the application of Mohr's circle of stress and material failure theories (such as Tresca's theory of stress) to alternative scenarios where the material is in bending, torsion, under axial load or in combinations thereof.

It is known that the properties obtained from uniaxial tension tests are a function of the strain rate used during a test. This phenomena is both true of metallurgical materials and for biological substances. For biological substances especially, this change in property is indicative of strain rate dependant molecular mechanisms that determine mechanical behavior. As an example of these molecular mechanisms, it was noted by Willett et al. (2007) that in a case involving high strain rate rupture of collagenous tissue, a large amount of visible recoil of fibers were seen. These fibers were theorized to suggest a build-up of elastic energy in a case where one would expect that sliding would dissipate this energy.

There are many facets of equipment that enable standard uniaxial tensile tension tests. The equipment must be highly rigid, it must be fitted with delicate instrumentation to measure force, deformation, time, and provide visualization of the sample. In the present case the equipment must enable a relatively high strain rate be achieving large velocities in short periods of distance (and thus time).

The design presented in this report overcomes strain rate limitations inherent with the currently employed hydraulically actuated model. The design overcomes this limitation at the sacrifice of other features on the present device that are not required in the research being conducted by the client. Such features include the ability to conduct biaxial tests.

Specifically, the Loading Apparatus for High Velocity Tissue Rupture (LAHVTR) was designed to fracture a specimen of bovine tendon (up to 2.5cm) at a strain rate of $1000s^{-1}$, recording force, position, and velocity (vs. time) as design criteria dictated.

This report outlines the progress of the team on the design, construction, and testing of the device. The brainstorming sequence surrounding the flywheel design, the final CAD drawings for the design, biological sample test results, a Gantt Chart, a final budget, and a description of the progress of the design unto completion are outlined in the report.

Team 12 is comprised of 4 members: Geoff Beck, Ben Breen, Ruth Domaratzki, and Rachael Schwartz. Our supervisor is Dr. Marek Kujath, and our client is Dr. Michael Lee of the Dalhousie Biomedical Engineering Department.

1.2 Tissue Mechanics

Research into the mechanical behavior of tissue allows for better understanding of failure mechanisms, which can influence treatment of such tissues. Research into impact loading of tissue could provide valuable information on the behavior of the collagen and elastin at a molecular level. Currently few institutes are performing such research.

Collagen is the most common protein in the human body, making up 60% of its dry weight (Lee, 2010). Collagen fibrils are secured by means of both intra, and inter molecular bonds (Figure 1).

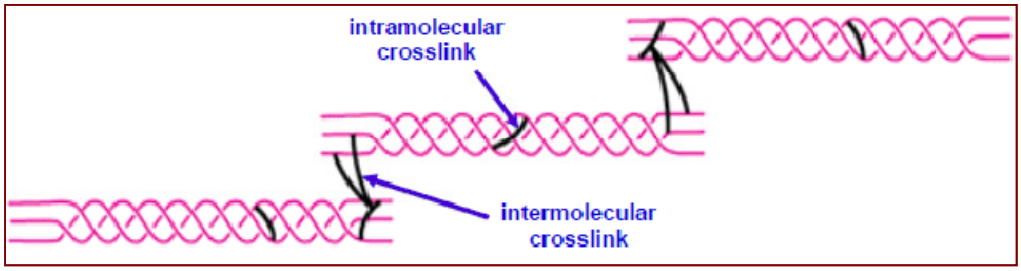

Figure 1: Crosslinking of Collagen Fibers (Lee, 2010)

The crosslinking presented above increased fibril; elastic modulus, tensile strength, and toughness (Lee, 2010).

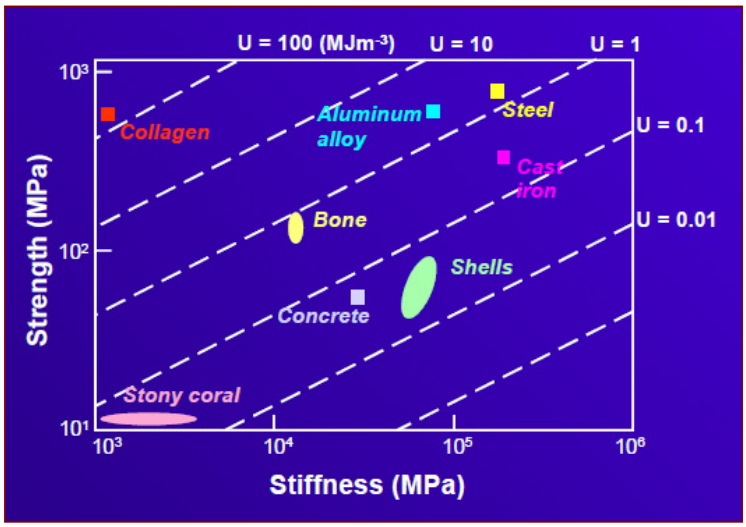

Figure 2: Strength and Stiffness Relationships for Materials (Lee, 2010)

The properties of collagen are somewhat surprising in that its strength is on the order of almost 10^3Mpa (which is similar to steel and aluminum alloy). Its stiffness however, is

lower (around 10^3Mpa) in comparison to other materials (steel is on the order of 10^5Mpa).

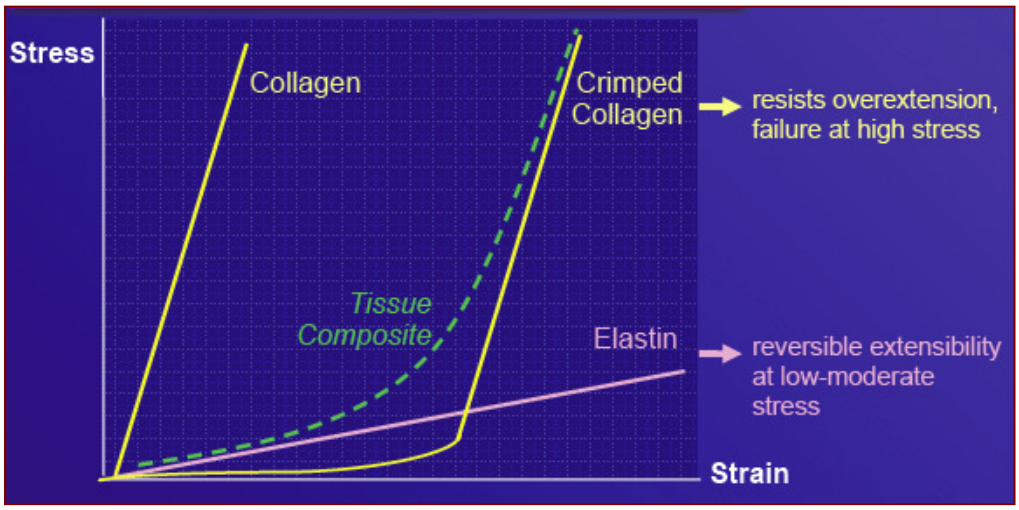

Figure 3: Structural-Mechanical Relations in Soft Tissues (Lee, 2010)

Elastin is a protein polymer similar to collagen, but with more elastic properties. The mechanicals properties of both collagen and elastin are presented in Table 1.

Table 1: Mechanical Properties of Collagen and Elastin (Lee, 2010)

Fibers	Elastic Modulus (MPa)	Tensile Strength (MPa)	Ultimate Elongation (%)
Collagen	1000	50-100	10 (crimped)
Elastin	0.6	1	100

Researchers have been fascinated by the performance of composite tissues such as tendon, ligament, skin, and arterial tissues. These tissues are composed of differing percentages of both collagen and elastin, and therefore exhibit differing behaviors as shown in Figure 3. The content and mechanical properties of some soft tissue composites are presented in Table 2.

Table 2: Content and Mechanical Properties of Soft Tissue Composites (Lee, 2010)

Material	Collagen (% dry weight)	Elastin (% dry weight)	Tensile Strength (MPa)	Ultimate Elongation (%)
Tendon	75-85	< 3	50-100	10-15
Ligament	70-80	10-15	50-100	10-15
Skin	60-80	5-10	1-20	30-70
Aorta	25-35	40-50	0.3-0.8	50-100

2 Objectives

The design requirements for the apparatus were agreed upon and were presented within the design memorandum as follows:

- The device will be mounted on a table top with one face approximately 30x30 in.
- Strain rates achieved will be on the order of $1000s^{-1}$
- The device should function approximately 5 years.
- The conditions of the test sample will be as close as possible to physiological conditions (100% humidity at 37˚C).
- The device will be designed so the operator has control of the extension rate.
- The device will be designed for safe operation performed by trained individuals. A shielding component will be incorporated if required.
- Accompanying the device will be a comprehensive instruction manual.
- All set deadlines and time requirements set out in the MECH 4010/4020 Design Project Handbook will be met.
- The device will attempt to provide data describing the force and displacement against time for each trial.

The design memorandum, design agreement and memorandum are located in Appendix A of this report.

Table 3: Design Requirements Check list

Design	Requirements	Accomplished
Size	30 x 30 inches	Yes
Strain rate	On the order of $1000s^{-1}$	No
Loading	Minimum 1/100s	
Life	5 years	Yes
Conditions of the test sample	Physiological conditions (100% humidity at 37˚C).	No
Safety	-Instruction manual -Shielding component	Yes

Data	- Force - Displacement	Yes

The team produced a memorandum document in which the agreed design requirements were outlined. The client and Team 12, before the design process begun, signed the document. The following subsections profile the design requirements and discuss the level of our accomplishments.

Size

The device should be able to fit on a tabletop with one face approximately 30X30 cm. The client presented this design requirement because he wanted to install the device on a laboratory counter in the Biological Tissue Testing Lab. The final apparatus measures 23X22 cm.

Strain Rate

The strain rate achievable should be on the order of 1000s^{-1}. The velocity of the moving grip is modeled as instantaneous. A sample of the length 0.8cm was tested and the velocity of the moving grip was measured to be 6.5 m/s. Using these variables, the strain rate was found to be:

$$\varepsilon' = \frac{v}{l_o}$$

$$\varepsilon' = \frac{6.5\,m/s}{0.008m}$$

$$\varepsilon' = 814 s^{-1}$$

The maximum strain rate reached by the LAHVTR is 81% that of the design requirement.

Loading

Achieve a minimum of 1ms loading. A confirmed loading was 4m seconds.

Lifetime

Should last approximately 5 yrs. The LAHVTR is created from sturdy components with overall robust design considered in every developing decision. Spare critical components were machined for the client. This design requirement was met.

Conditions of Test Sample

The conditions of the test sample will be as close as possible to physiological conditions (100% humidity at 37˚C). Used spray bottle to keep sample at conditions while loading and unloading sample

Control

The device will be designed so the operator has control of the strain rate. Using the frequency controller and the stroboscope, the operator has control over the velocity of the

device and therefore, the operator has control over the strain rate. This design requirement was met.

Safety
The device will be designed to be safely operated by trained individuals. A shielding component will be incorporated if required. The device operated well within safe operating conditions. The device is designed to be operated by an individual that is trained by reviewing the operation and safety manual. Within this demographic, this design criteria is met. It became apparent during the design process that it was necessary to fit the LAHVTR with a polycarbonate safety shield.

Documentation
The device will be accompanied with a comprehensive instruction manual. The team achieved this requirement by completing an instruction manual for the operation of the device along with some safety recommendations. This manual is located in Appendix E.

Timing and Deadlines
All set deadlines and time requirements set out in the MECH 4010/4020 Design Project Handbook will be met. Throughout the year, Team 12 has met or exceeded all deadlines and requirements associated with the course work, deliverables, and testing.

Data Acquisition
The device should provide data describing the force, displacement, and time for each trial. This design requirement was met and the output from the device is discussed in detail in later sections. An LVDT and Bending Load Cell are incorporated in design and the data is processed using DAQ.

3 Generation of Alternatives

The following section presents two alternative designs that were considered and the benefits and the drawbacks of each design. The designs of this section were rejected with the accepted design presented following this section.

3.1 Hopkinson Split Bar Apparatus

The Hopkinson Split Bar apparatus (HSBA) is used extensively in materials testing because of its ability to achieve extremely high strain rates. The HSBA functions by propelling a striker tube (using a compressed air gas gun actuator) towards an incident bar. When the striker tube impacts the incident bar, a pulse wave is transmitted through the incident bar and into the sample. Some of the pulse wave is then reflected back through the incident bar (and captured in the momentum trap bar) and some is dispersed in the transmission bar. Using an Enhanced Laser Velocity System (ELVS), the deformation and velocity of the sample can be measured dynamically. This data would then be input into The DAC card to be analyzed and recorded. The HSBA is shown in Figure 5.

The main benefit of this design is that extremely high strain rates have been reported, additionally, the ELVS can attain the dynamic stress strain curve. However, there are several drawbacks of this design. Firstly, the gas gun raises several safety concerns, as extremely high pressures are needed to propel the striker tube. Additionally, the HSBA is difficult to calibrate, as pulse wave magnitude has to be finely tuned to the pressure the gas gun actuator. Finally, we foresee this device being expensive because the compressed air system needed for the gas gun and, incident and transmission bar have to be machined to very accurate specifications.

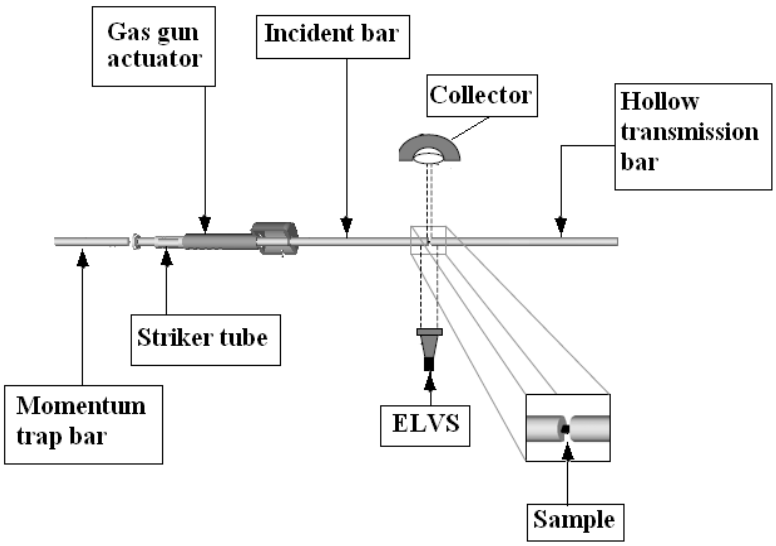

Figure 4: Hopkinson Split Bar Apparatus

3.2 Gravitational Impact Pendulum

A method of biological specimen testing biological specimens based on a gravitational impact pendulum was considered. Figure 6 outlines the core components of such a device. A pendulum-based approach has been employed in metallurgical testing to determine properties such as hardness, necessary modifications would be needed to meet the specifications set by the client. A pendulum-based design would be capable of meeting the objectives for lifetime, conditions, control and data acquisition as defined in our Design Memorandum.

The pendulum-based design however was considered likely to fail on the objectives of our chosen size and control criteria. A base size of 30in x 30in was deemed optimal for the laboratory setting of the device, and it was likely that the swing of such a pendulum would be capable of fitting within these dimensions while achieving the rate required. A pendulum approach was considered also to be susceptible to control issues as a mechanism for reproducibly determining required drop heights from requested strain rates was needed.

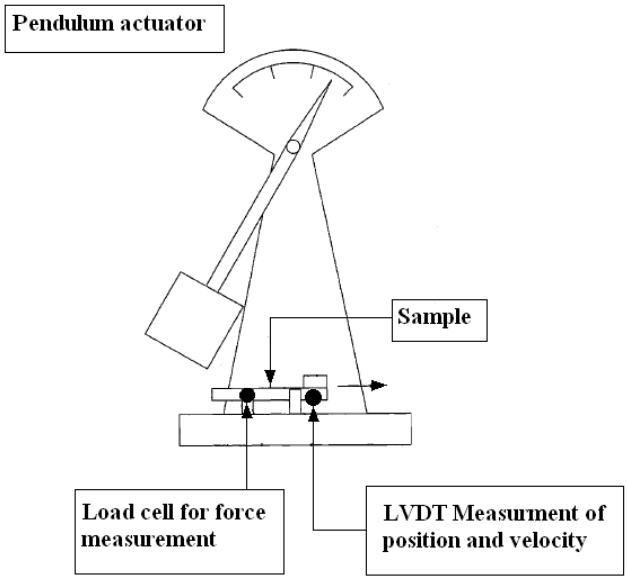

Figure 5: Gravitational Impact Pendulum

The gripping system will consist of corrosion resistant material. A corrosion resistant material is necessary because the biological specimen will be placed in a corrosive aqueous saline solution. It was suggested by the client that Polyacetel would be a preferable material due to its non-hydroscopic (not absorbing liquid) characteristic. If the material is to absorb liquid, the assembly may not come apart easily after long exposures to the liquid. The grips will be mounted on a track to eliminate buckling and restrict the strain to the axial direction.

4 Selected Design

The following section outlines our selected design and the mechanism that we used to select it from the alternatives.

4.1 Design Evolution

The selected design consists of several different operational sections. The device is broken down into the flywheel and motor, the engagement mechanism, and the gripping device sections.

The flywheel is a reasonable design due to its significant moment on inertia resulting in a storage device for rotational energy. This characteristic lends itself to be a useful device in controlling a constant velocity. The flywheel design was initially thought to be constructed out of stainless steel with an estimated diameter of twenty centimeters. The brushless motor will have variable speed capabilities so the operator may test under a range of speed variables and thus, strain rates. The engagement of the actuation method will be performed in response to an electrical signal generated by the data acquisition system.

Several methods for engaging the flywheel were under consideration. Initially, the design was thought to hold a lightweight weight engagement wheel that will not continue to rotate with the flywheel after the needed energy is removed from the flywheel with the use of a sacrificial part, electromagnetic engagement, and a clutch system.

The gripping system consists of corrosion resistant material. A corrosion resistant material is necessary because the biological specimen will be placed in a corrosive aqueous saline solution. The grips will be mounted on a track to eliminate buckling and restrict the strain to the axial direction.

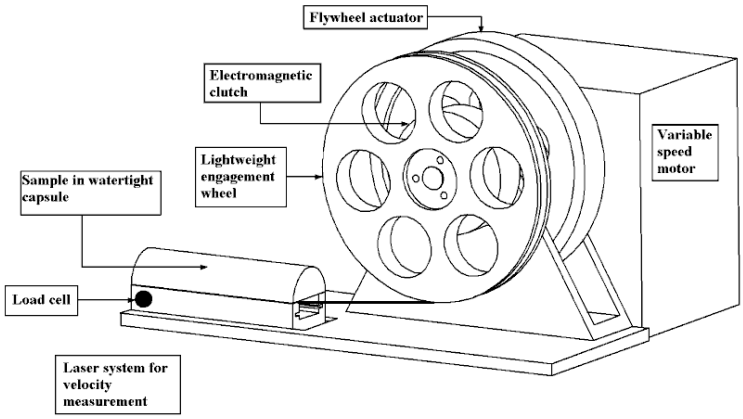

Figure 6: Early depiction of LAHVTR

Breaking the design into several sub-components, and listing the various solutions to these sub-components obtained from brainstorming sessions obtained the selected design. Next, reasonable combinations of design sub-components were listed as design solutions as shown in the morphological chart in Appendix B. Following this, the reasonable combinations were then ranked based upon criteria that were deemed integral to the design. From this ranking process, we were able to attain the three design ideas discussed in this report. Finally, the three designed were assessed using the House of Quality as shown in Appendix B.

The House of Design determined that the flywheel design satisfied the outlined criteria the most. The team supervisor and client accepted the flywheel design and the team began brainstorming more detailed design specifications.

The first design consisted of two flywheels and a clutch. One of the wheels held one side of the sample and does not rotate. The second wheel is stationary until the motor is at full velocity and the clutch is engaged to the flywheel, which breaks the specimen. This flaw in this design lies in the fact that having two wheels is unnecessary if the gripping mechanism is attached to the ground and the moment of inertia of the flywheel is not being utilized.

The next design consisted of the gripping mechanism situated on the tabletop to enable the filming of the specimen breaking with a high-speed camera. The flywheel was connected to the motor and when the flywheel reaches the needed velocity an electromagnetic clamp engaged the flywheel. This would pull a cable that is attached to the gripping apparatus. This design was not chosen because a mechanism could not be sourced that could grip the flywheel quickly enough to get up to the velocity needed to break the specimen.

4.2 Design Selection Matrices

Breaking the design into several sub-components and listing the various solutions to these sub-components obtained from brainstorming sessions resulted in design selection. Next, reasonable combinations of design sub-components were listed as design solutions as shown in the morphological chart in Appendix B. Following this, the reasonable combinations were then ranked based upon criteria that were deemed integral to the design. From this ranking process, we were able to attain the three design ideas discussed in this report. Finally, the three designed were assessed using the House of Quality as shown in Appendix B.

5 Problem Exploration

In order to more clearly understand the intricacies of the design and conceptualize the requirements, the team completed research and testing on several aspects of the design. Initial testing was conducted to determine the validity of the engagement mechanism and solenoid operation. A mock-up of the device was constructed to determine the optimal placing of members and a rapid prototyped model was created to confirm the final dimensions of the device.

5.1 Modeling

Several methods of modeling were performed to aide in the conceptualization of the device, determination of high stress areas, and the dimensions of the engagement mechanism with respect to the flywheel.

5.1.1 LAHVTR Mock-Up

First a mock-up of the device was constructed to help the team conceptualize the aspects of the design that required revision. The mock-up additionally enabled the group to foresee the initial placement of the components around the flywheel. The model was constructed from Foam core and wooden dowels.

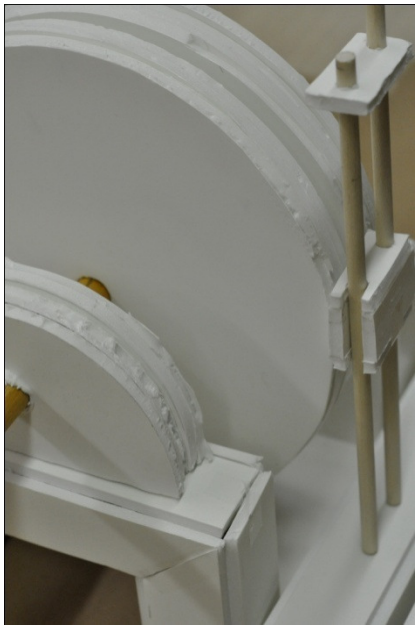

Figure 7: Mock-up of Device

5.1.2 Finite Element Analysis

Preliminary finite element analysis was applied to the flywheel to find the range of stress concentrations in the contact area of the flywheel. This initial analysis is represented as a point load and depicted in Appendix C. The team discussed the utilization of modeling a more precise finite element analysis model for the completion of the final design but the concept was passed over due to lack of usefulness.

5.1.3 Rapid Prototyping

Representations of the engagement mechanism and flywheel were created using rapid prototyping. These components were then precisely mounted on a wooden frame to determine the validity of the design concept and finalize the dimensions of the apparatus.

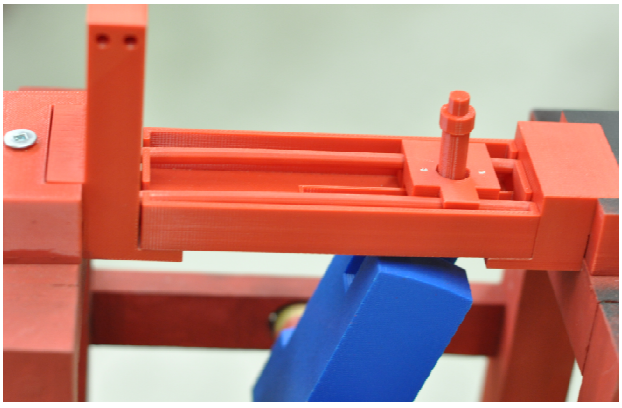

Figure 8: Rapid Prototype of Device

5.2 Testing

Some rudimentary tissue testing was conducted prior to construction of any device to aide in problem exploration.

5.2.1 Biological Specimen Testing

Initial testing was performed on the Loading Apparatus for High Velocity Tissue Rupture to verify the successful operation of the engagement mechanism. Biological tissue was loaded into the LAHVTR clamps and the pin was manually engaged through the circuit board. Testing was performed with the flywheel at four speeds. Table 4 outlined the information gained during the testing.

Table 4: Biological Specimen Testing Results

Test	Flywheel Speed [rpm]	Successful Engagement Mechanism Employment	Observations
1	300	Yes	No wear
2	500	Yes	Engagement pin surface chip
3	700	Yes	Engagement pin surface chip
4	1000	Yes	Engagement pin deformation

5.2.2 Solenoid Testing

The solenoid was tested under several applied voltages to determine the time encountered when fully extending the solenoid core. This time period was then compared against the necessary time period needed to successfully engage the pin with the flywheel. Five trials were performed and the average of the data was recorded. Figure 9 compares the experimental to the theoretical data of applied voltage to time encountered for full extension of the solenoid core. The obtained data shows that the solenoid is well within the needed operating range for the task of engaging the pin to the flywheel.

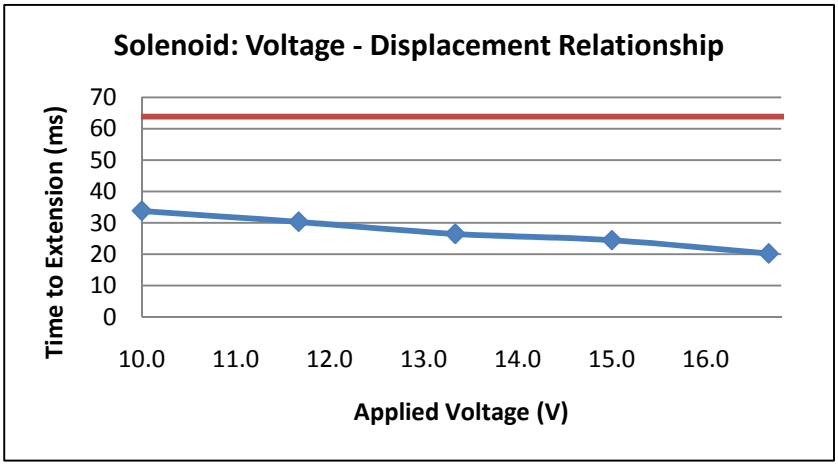

Figure 9: Solenoid voltage vs Time (theoretical-red, experimental-blue)

6 Calculations

A valid concern about the flywheel driven impact apparatus was its ability to provide an acceptable output displacement profile. An acceptable profile has constant strain rate past the transient period and a transient period of no more than one-fourth the fracture strain[1]. This document seeks to provide an assurance that an acceptable profile will be attained. Figure 10 attempts to illustrate both an acceptable strain rate profile and the anticipated profile which has been obtained from our calculations that follow.

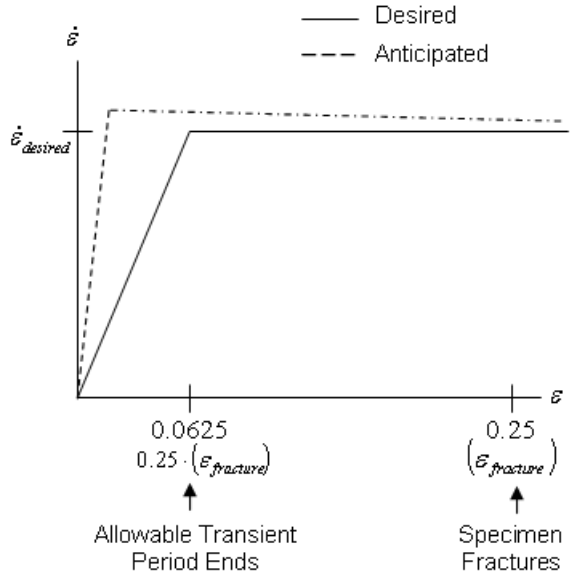

Figure 10: Desired vs Anticipated Strain Rate

[1] Meeting, 30th September 2009.

In this scenario the motor is disconnected from the inertial load (flywheel) through the use of an overrunning clutch. To the end of obtaining the profile, the principal of inelastic impulse and momentum is applied. The properties of the flywheel (w) and specimen grip (g) are selected to be:

$$m_w = 16\ kg$$
$$m_g = 1\ kg$$
$$d_w = 20\ cm$$
$$I_w = 0.061\ kg \cdot m^2$$
$$\omega_{w,1} = 100\ rad/s$$

Conservation of angular momentum (about point A, the center of flywheel rotation) results in the expression:

$$(H_A) = (H_A)_2$$
$$I\omega_1 = I\omega_f + m_g v_g r$$
$$(0.061\ kg \cdot m^2)(100\ rad/s) = (0.061\ kg \cdot m^2)\omega_f + (0.1\ kg \cdot m)V_{g,2} \quad (1)$$

The result is one equation with two unknown quantities. An additional bit of knowledge is needed in this case. The coefficient of restitution, a function of the material in impact, is applied. This coefficient relates the velocities of the masses along the line of impact, just before and after the collision (Hibbeler, 2007). This coefficient, for steel, is $e = 0.95$ but is susceptible to both changes in geometry and surface hardening.

$$e = \frac{V_{g,2} - V_{w,2}}{V_{w,1} - V_{g,1}}$$
$$e = \frac{V_{g,2} - r\omega_f}{r\omega_i}$$
$$0.95 = \frac{V_{g,2} - r\omega_f}{(0.1\ m)(100\ rad/s)} \quad (2)$$

Solving (1) and (2) results in the following:

- a final grip velocity of 16.75 m/s.
- a final grip kinetic energy of 140 J.
- a flywheel angular velocity of 72.5 rad/s.
- a final flywheel kinetic energy of 160 J.
- energy losses of 11 J.

These answers coincide strongly with solutions obtained through the application of the "Working Model" software package with errors (in terms of energy) of less than 7%.

Friction and the load posed by the sample are thought to have no effect on the motor of the grip. The following calculations highlight this reasoning.

For the load, assuming the specimen to be spring-like, we were told that the breaking force was 15 N at a length of 3mm, so the spring constant is about (with a safety factor) 10000 N/m. This generalization is likely weak. The energy dissipated in a stretch to breaking for the specimen should be about 0.045 J. These calculations follow below (with an additional safety factor present for strain distance - Δx is said to be the maximum elongation of the specimen).

$$k = \frac{15\ N}{0.003\ m}(SF) = 10000 N/m \tag{3}$$

$$E_{lost-(specimen)} = \frac{1}{2}k(\Delta x)^2 = \frac{1}{2}(10000 N/m)(SF \cdot 0.003)^2 = 0.5\ J \tag{4}$$

The frictional losses are based upon the coulomb model for a $\mu_k = 0.3$ which is common for steel-on-steel surfaces without lubrication. The losses due to friction and (work against gravity in the vertical configuration) are expected to be about 0.5 J and are presented below.

$$E_{lost-(friction)} = \mu F_n(\Delta x) = 0.3 \cdot (1\ kg \cdot 9.81\ N/kg \cdot SF) \cdot (0.003\ m \cdot SF) = 0.2\ J \tag{5}$$

$$E_{lost-(gravity)} = mg(\Delta x) = (1\ kg \cdot SF) \cdot (9.81\ N/kg) \cdot (0.003 \cdot SF) = 0.3\ J \tag{6}$$

The mass of the grip (1 kg) and its velocity at impact provides for more than adequate amounts of kinetic energy to overcome friction, gravity and the specimen without appreciable changes to its velocity.

The amount of time to reach the desired velocity following impact is determined from the following expression where σ is the speed in sound within the material (for steel = 5000 m/s)[2]:

$$\Delta t = 2\frac{L}{\sigma} \tag{7}$$

The time was found to be $6\ \mu s$ for a pin of 2 inches in diameter. Since the pin is of less than this diameter the value for this "ramp time" is surely less than any maximum acceptable value.

Due to the variable nature of the coefficient of restitution it is only through experimentation following the build of a prototype that a solid relationship between the

[2] http://tinyurl.com/yea2xt4

flywheel rate of rotation and the linear velocity of the specimen grip may be determined.

However these calculations show:

- that the desired velocity (and thus strain rate) will be obtained in the transient region.
- that the resulting displacement profile should be free of large decelerations in the time leading to fracture.
- and that a solid relationship between ω and e exists through an experimental determined quantity e.

Calculations were performed regarding the torque that the shaft was subjected to. With these results, the team designed the method of connecting the flywheel to the shaft. The team plans to improve on the gripping mechanism performance by researching methods of decreasing the mass of grip that undergoes linear motion upon impact.

7 Final Design

The second term of this design project allowed for refinement of the original design and the implementation of the measurement systems. The final design is presented in Figure 11. This section will detail the system in terms of both mechanical components and measurement/control systems.

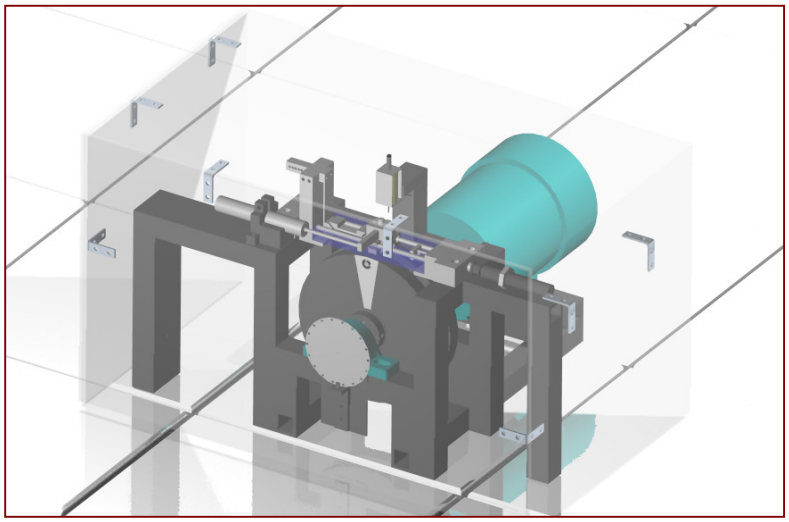

Figure 11: Final Design

7.1 Drive Shaft Assembly

The drive shaft (Figure 12) assembly of this system consists of a flywheel which is driven by a 3 phase motor (more specs) under frequency control. The drive shaft is coupled to the flywheel shaft by means of a flexible spider coupling.

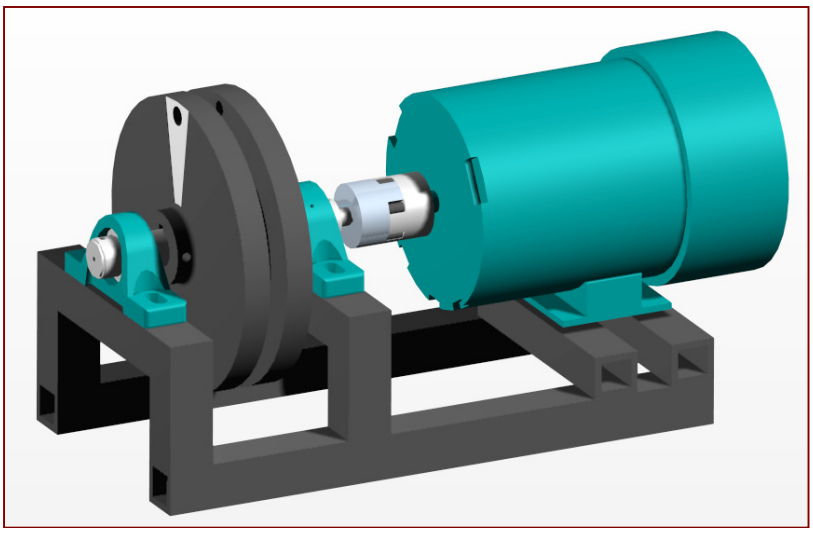

Figure 12: Drive shaft Assembly

7.1.1 Flywheel Design

When designing the flywheel the mass, size, and the cost of the flywheel were the main considerations. Increasing the mass, increases the moment of inertia that increases the available energy that is available for transfer to the specimen during impact. The design utilizes this energy (and the subsequent force) to accelerate the gripping mechanism that fractures the specimen.

The flywheel is machined out of 0.2 m diameter carbon steel. This material was chosen for it's low cost and high weight. It is also a common material that can be ordered locally which will reduce the cost further. The flywheel was modeled after a disc of uniform thickness. The failure calculations show the flywheel will not fail at the intended angular velocity of the shaft. These calculations are located in Appendix C.

The flywheel was designed with flanges to decrease stress concentrations of the flywheel at the critical areas for shear stress. Tresca's theory of failure was used to find the maximum shear stress. The flanges are not included in the failure calculations of the flywheel though they add a factor of safety to the design. The diameter of the flywheel is sufficient such that, the arc of motion needed to fracture the tissue can be modeled as approximately linear.

Figure 13: Flywheel

Figure 14 is a plot of the flywheel diameter (series2, constant thickness of 5cm) and thickness (series1, constant diameter of 20cm) versus the flywheel mass. The plot used a density of carbon steel for calculations. This graph was created to give Team 12 an understating how the flywheel mass changed with changing dimensions. This was a valuable tool that helped select the flywheel dimensions as the team could quickly see the effect of changing parameters.

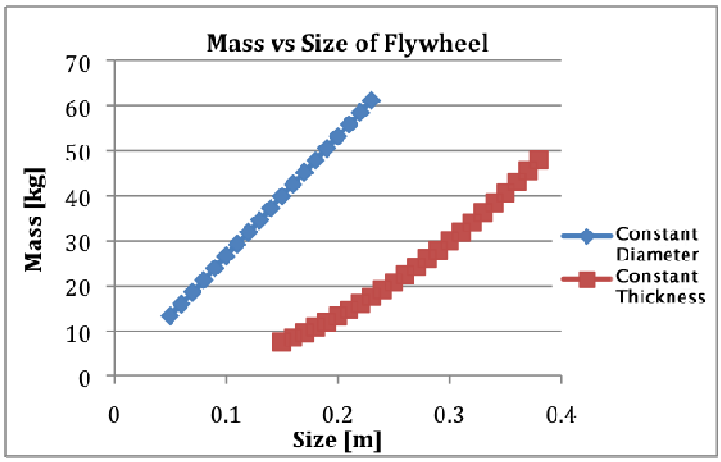

Figure 14: Flywheel Design

The flywheel is fitted with a pin (Figure 15) that contacts the actuating pin on the gripping mechanism. This pin and actuating pin are constructed from carbon steel. This material is hard and strong and holds low ductility. These characteristics are necessary for the high impact loading presented to these items.

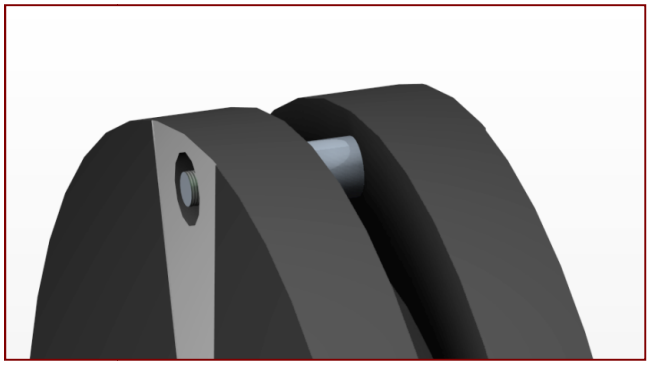

Figure 15: Engagement Pin in Flywheel

7.1.2 Main Shaft

The main shaft to which the flywheel will be mounted is constructed of carbon steel; it is to be one inch in diameter and eight inches long. The choice to construct the shaft of carbon steel was a budgetary decision. The shaft was a donation from the Mechanical Engineering Department.

Furthermore, constructing the shaft with a one-inch diameter was deemed ideal because the static shaft deflection from the flywheel was calculated to be negligible at this dimension. Additionally, the critical shaft speed was calculated to be approximately 12 times the operating speed of 955 rpm. Figure 16 illustrates an exploded view of the drive shaft assembly.

Lastly, Team 12 is considering different methods to couple the motor to the main shaft. The team chose a flexible coupling due to its vibration management capabilities and ease of alignment.

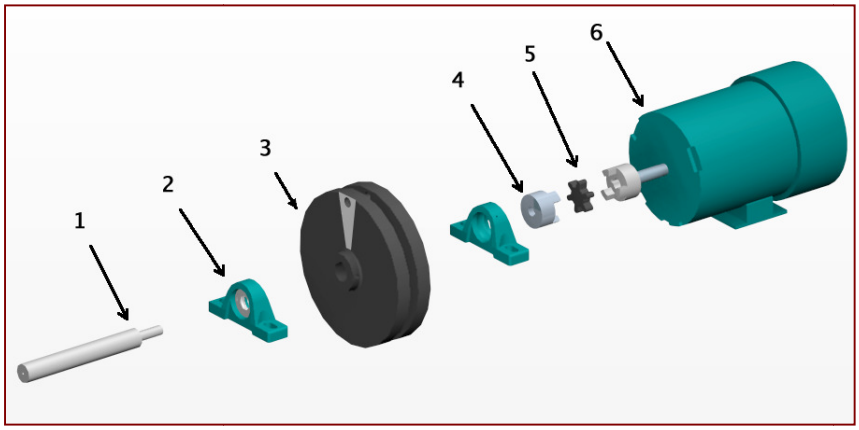

Figure 16: Exploded View of Drive Shaft Assembly

Shaft [1], Bearing [2], Flywheel [3], Coupling [4],
Spider coupling joint [5],and Motor [6]

7.1.3 Gripping Mechanism

The gripping mechanism consists of two grips that hold the sample at each end, a linear sliding track, and support housing for bearings and the contact tooth. The grips are machined out of stainless steel. One side will be attached to the force transducer while the second end is attached to housing, allowing it to move down the sliding track. The housing is machined from a stainless steel. The contact tooth will be designed using the same carbon steel as the flywheel pin. Figure 17depicts an exploded view of the grip assembly.

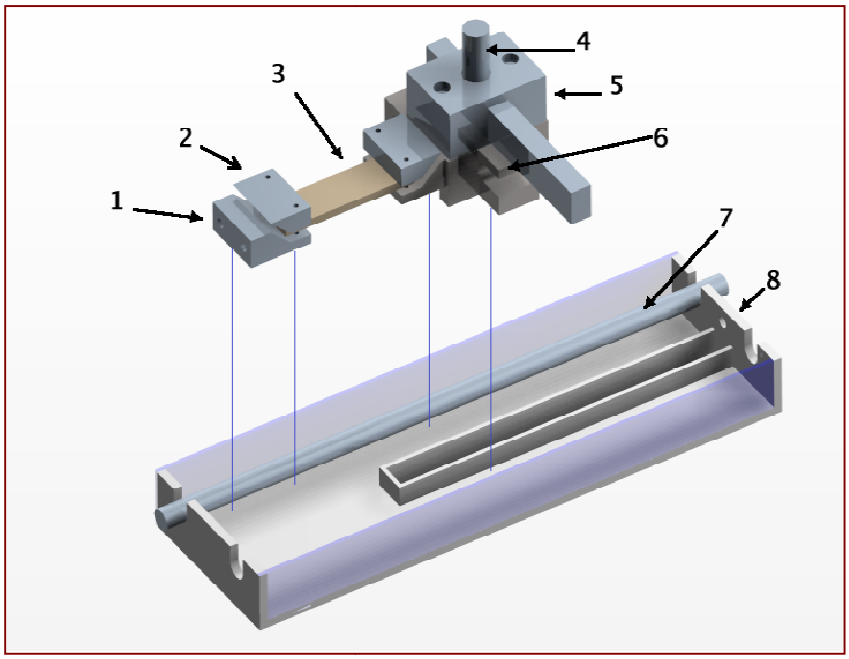

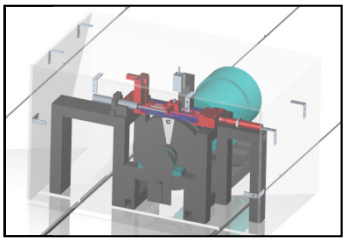

Figure 17: Exploded Grip Assembly

Grip [1], Grip top [2], Specimen [3], Engagement pin [4],
Tooth holder [5], Tooth housing [6], Guide rod [7], Bath [8]

7.1.4 Damper

The team estimated the forces involved in the operation of the engagement mechanism. A pre made damper was sized using these calculations and purchased. This damper was fastened on the end of the track to deter the tooth housing from rebounding and distorting the sample.

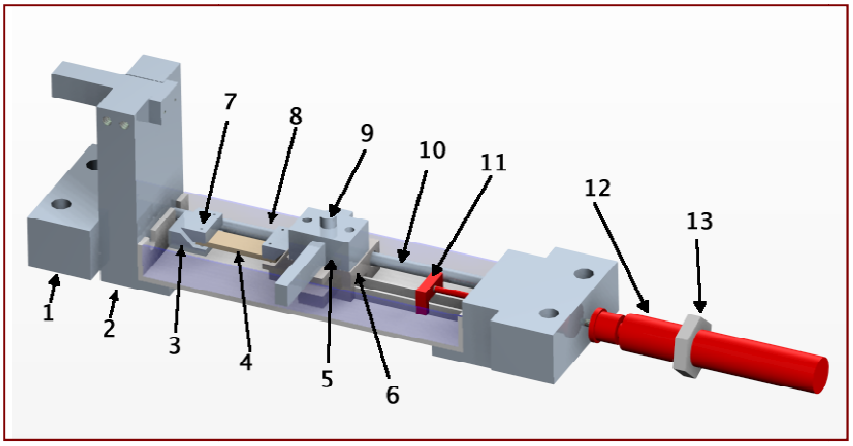

Figure 18: Damper set-up

Engagement mechanism support [1], Force transducer [2], Grip [3], Specimen [4], Tooth holder [5], Tooth housing [6], Grip top [7], Bath [8], Engagement pin [9], Guide rod [10], Damping system[11], Damper [12], Mounting nut[13]

7.1.5 Safety Shield

Due to high rotational speeds and large impact forces, the device is enclosed in a safety shield. The safety shield is to be constructed out polycarbonate panels to aid in the ability to view the flywheel operation. The safety shield is depicted in Figure 11.

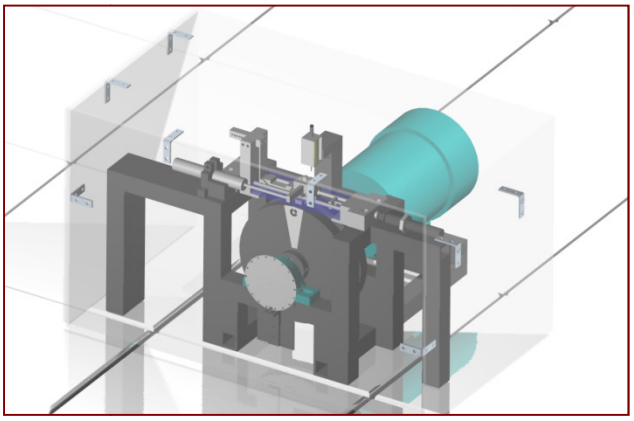

Figure 19 - Diagram of Safety Shield

7.2 Electrical Components

The electrical components of this project consisted of a motor and frequency drive, the measurement systems, DAQ system, and high-speed video camera equipment.

7.2.1 Motor and Frequency Drive

The device is driven using a 1/3 horsepower, 115-volt, three phase, AC motor; controlled using an AC Drive. The motor was selected on its ability to drive the flywheel at 1000rpm and operate using a standard 115-volt power supply. An AC motor was selected over a DC motor based on cost and ease of power supply.

Additionally, the frequency drive was selected based on its ability to easily and accurately control the motor frequency (speed). Furthermore, the drive is compatible with a PC computer, thus if the client prefers, the motor can be controlled from a PC.

Figure 20: Frequency Controller

7.2.2 Measurement Systems

The measurement systems are all controlled through the DAC card. The operator initiates the rotary encoder through the PC. The rotary encoder senses the position of the flywheel and the solenoid is automatically deployed and the data requisition system is initiated to collect the data.

7.2.2.1 Rotary Shaft Encoder

The pin is engaged (and consequently the specimen is loaded) both after the flywheel reaches the desired speed and after the pin is in the precise location. Inability to locate the pin could result in partial contact of the impacting surfaces and failed experiment and destroyed specimen. A rotary encoder is mounted on the shaft and acts as a signal to engage the solenoid.

The encoder is an infrared sensor that senses light passing between two sensors on either side of the encoder. Only one hole is necessary on the rotary encoder. The computer driver for the tissue rupture device was developed to allow for the pin to fire after activation of the 'fire' button and completion of the revolution of the flywheel. This allows for a failsafe method, ensuring the pin will never miss fire.

7.2.2.2 Stroboscope and Frequency Controller

The angular velocity of the flywheel determines the strain-rate experienced by the specimen. The strain-rate is a controlled quantity thus measurement of angular velocity is required. The Strobotac is used to determine the angular velocity of the flywheel in operation by adjusting the frequency controller until the white stripe painted on the flywheel appears to be in a constant position. The frequency controller displays the speed of the flywheel in RPMs while the shaft is rotating.

7.2.2.3 Force Transducer

A standard strain gauge will be mounted to a titanium component on the device. This configuration will permit measurement of force loading on the specimen. This is illustrated in Figure 21. Calibration of the force transducer is required. The team measured the voltage change as a result of the application of several calibration weights. These output points were then used to determine a linear relation between the deflection and voltage change. This relation is used to determine the force applied to the specimen. The results of the calibration are discussed in the calibrations section of this report.

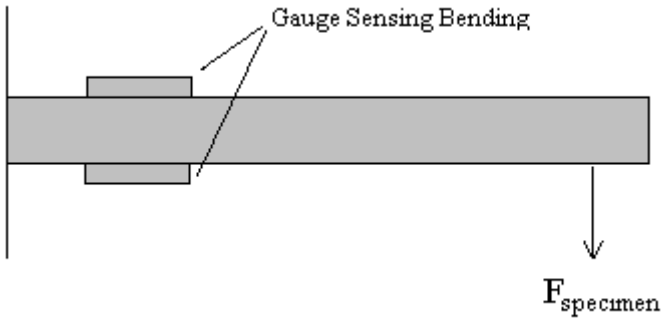

Figure 21: Specimen Force Measurement

The force cell was selected based on several criterions. Firstly, the strain gauges were selected based on the theorized forces and other characteristics that would ease mounting the gauges. The size and material of the load cell was determined. Titanium was selected for its relatively low Young's modulus (approximately half that of steel) because the project forces were thought to be approximately several hundred Newton's (based on information obtained from the client). Furthermore, the nominal length and width were fixed as a result of geometry. Therefore, working gauge length and cell width was used to create a scenario that would result in strains that were compatible with the selected gauges. The working gauge length was selected to be five centimeters; this was mainly chosen for practicality reasons. Lastly, the thickness was based on available titanium sizes, several thicknesses were considered, however, 2 millimeters yielded the best results based on the equation below:

$$\epsilon = \frac{Px}{Ebt^2}$$

Where P is the force, x is the working gauge length, E is Young's modulus and t is the cell thickness.

Therefore, bases on the numbers described above, the strain was calculated to be 1700με which was well within the selected gauge specifications.

In terms of actual data measurement, the voltages were collected using a Wheatstone bridge and amplified using a load cell amplifier. Similar to the other measurement devices, the data was input into a PC via a DAQ card and processed using software.

The two gauges were placed into a Wheatstone bridge configuration as per Figure 22 with Rx = Ra = 350Ω and Rm = Rm = 350 Ω strain gauges.

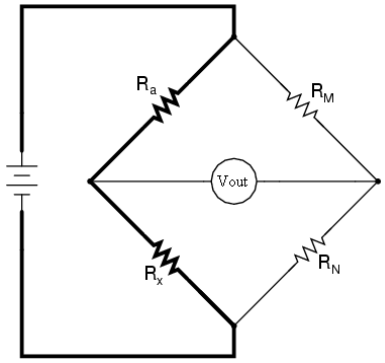

Figure 22: Wheatstone Bridge Configuration

7.2.2.4 Linear Variable Displacement Transformer

As the core of the Linear Variable Displacement Transformer (LVDT) moves, the output voltage increases from zero to a maximum. The magnitude of the output voltage is proportional to the distance moved by the core. This output voltage is collected by the DAC card, converted to distance (using calibration curves), and displayed in a graph of voltage vs. time and distance vs. time.

7.2.3 Solenoid Actuation

The actuation of the contact tooth was conducted using a solenoid. The solenoid is controlled through The DAQ card to enable precise deployment. Figure 13 depicts the contact tooth in the initial position. The contact tooth will remain in this position until the flywheel reaches the appropriate angular velocity. At that point, the technician will activate The DAQ card and the solenoid will push the contact tooth into the final position. In this position the contact tooth will meet the flywheel pin. The flywheel pin will move the contact tooth, along with the grip, along the track. This motion will rupture the tissue. The second position is also depicted in Figure 24 and **Error! Reference source not found.**.

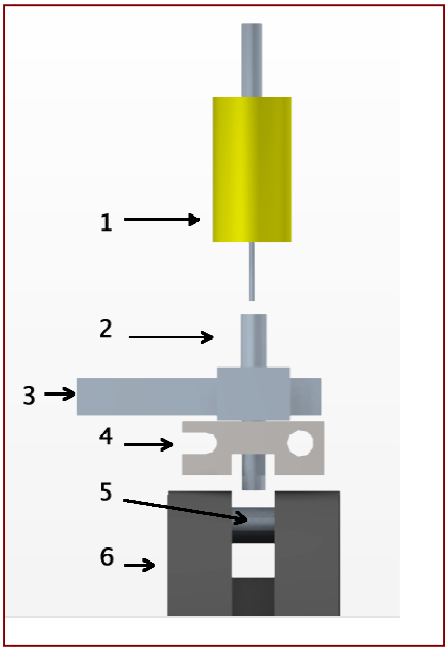

Figure 23: Initial Position of Contact Tooth

Solenoid [1],Contact tooth [2], Tooth holder [3], Tooth housing [4], Pin [5], Flywheel [6]

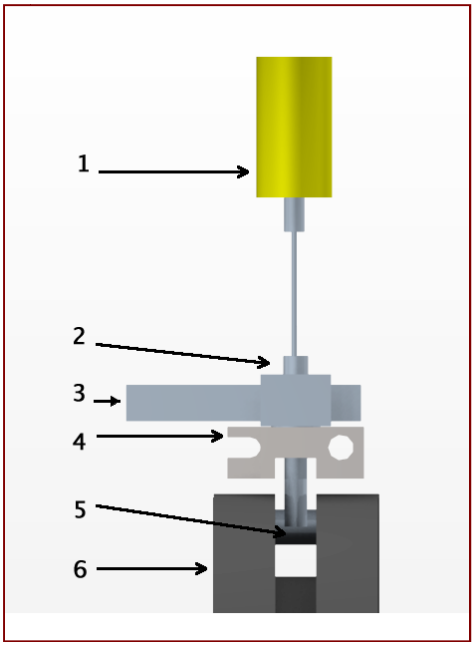

Figure 24: Final Position of Contact Tooth

Solenoid [1], Contact tooth [2], Tooth holder [3], Tooth housing [4], Pin [5], Flywheel [6]

8 Implementation of Measurement Systems

8.1 *Calibration of LVDT*

Figure 25, below shows a calibration curve for the LVDT. This was generated by measuring the voltage at known distances from the starting position. The data was then correlated using a linear regression to project the measured voltage to a given distance. If one notes the R^2 value of 0.9982, the data is almost a perfect fit.

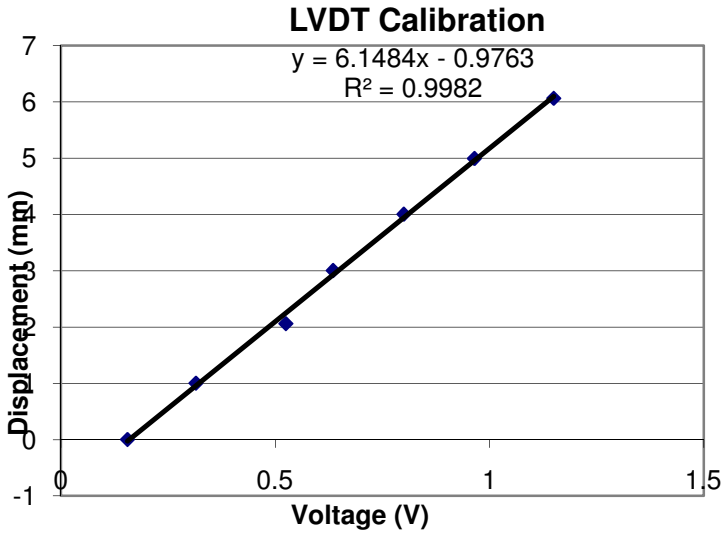

Figure 25: Calibration Graph for LVDT

8.2 *Calibration of Force Transducer*

The calibration of the force transducer was done in a similar fashion to the LVDT. Known masses were hung from the load cell and voltages were recorded. The masses were then multiplied by the acceleration due to gravity to get the force applied. Again the data was fit using a linear regression and is shown in Figure 26. Once again note the nearly perfect linear match with an R^2 value of 0.9991.

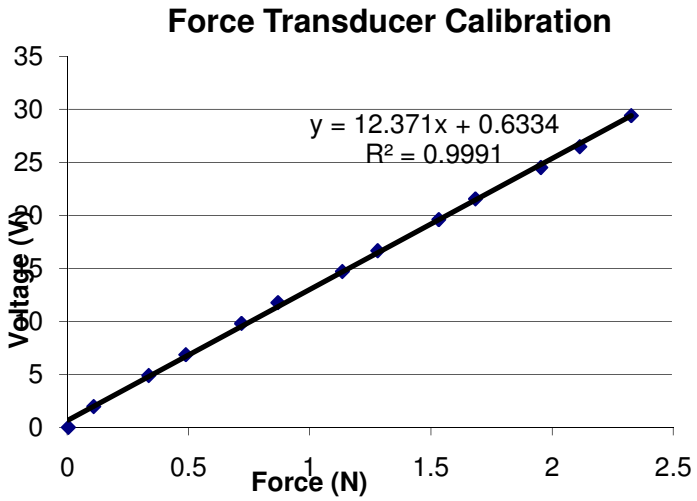

Figure 26: Calibration Graph for Force Transducer

9 Safety

During the design process creating a safe device was of the utmost importance. Therefore, we considered three levels of safe design, including; procedural safety, engineered safety and inherent safety.

Firstly, for procedural safety, Team 12 wrote an operation manual. This operation manual outlines safe operation of the device as well as clearly outlining the risks and hazards associated with device operation. Secondly, we encased the device in a safety shield constructed of polycarbonate panels. This will ensure the operator is safe should the device catastrophically fail. Lastly, the design we have created is inherently safe because the operator can control the device remotely from a computer, away from the actual device. Safety precautions are outlined in the User's Manual in Appendix D.

10 Testing

The following sections outline our testing procedure, our methods of validation, and the data that we were able to collect.

10.1 Test Procedure

1. The specimen is sized and placed in specimen grips.

2. The specimen is placed in pretension by adjustment of the force transducer. The Allen key tightens the setscrews at the desired tension.

3. The zero position of the LVDT in the centre of the throw so centre the initial position around the centre of the entire throw to obtain the most accurate results.

4. Place the safety case over the flywheel section.

5. Turn on the Stroboscope and set the RPM dials to the desired angular speed.

6. Turn on the frequency controller and gradually increase the speed until the white stripe on the flywheel appears to be stationary. This indicates that the angular speed of the flywheel is the same as the displayed angular speed on the stroboscope.

7. Press enter to record the data.

10.2 Validation Method

The LVDT and the force transducer were calibrated to aide in verifying the method used. While the machine is stationary, the voltage output for several distances was rerecorded and these points were used to create a calibration curve. The device is activated and the output data from the test is compared to the calibration curve to verify the validity of the data.

Furthermore, the LVDT was validated using a high speed camera and video processing software. Testing was recorded using video capture at 500 frames per second. The acquired video was then processed and the software was able to match image points in several frames over time and output velocities and positions.

Additional validation of the load cell was considered. This potentially could be completed using the video processing software. On the video one can track how the load cell moves linearly when the sample is stretched. Using this information in addition to the properties of the cantilever load cell (length, height, width, material) and can calculated the required force to move the load cell the distance calculated in the video software. Given the high R^2 value of the load cell, this additional validation was deemed unnecessary.

10.3 Measurement Equipment Testing Results

When tested the signals of Figure 27 were acquired.

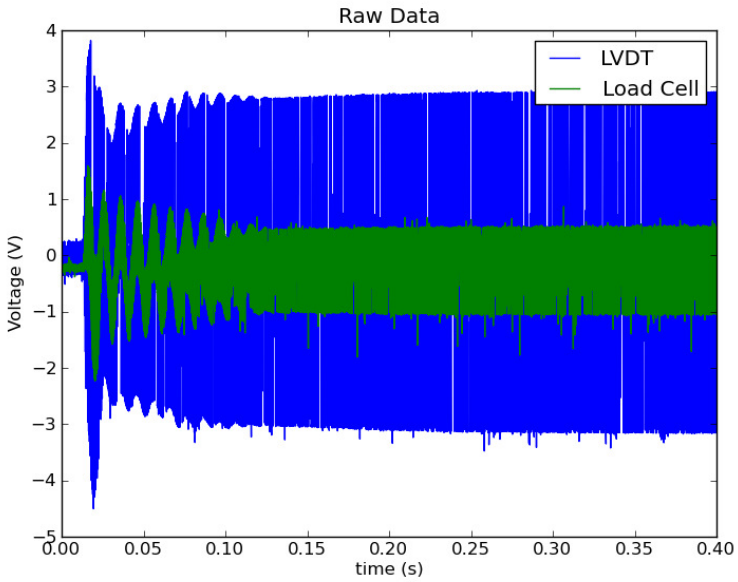

Figure 27: Raw Signals Acquired During Testing

The signals were processed and are presented in processed form in Figure 28. The root-mean-square of the LVDT signal was taken for each half-period and then multiplied by $\sqrt{2}$ because $V_{peak} = \sqrt{2}V_{rms}$. Label "A" of the figure indicates the action of the gas spring. Label "B" indicates a region of constant velocity over a long distance of travel. Label "C" indicates that the specimen displaced before it strained and that the sample was likely under-tensioned. Label "D" indicates resonance of the beam which was easily seen under high-speed video analysis.

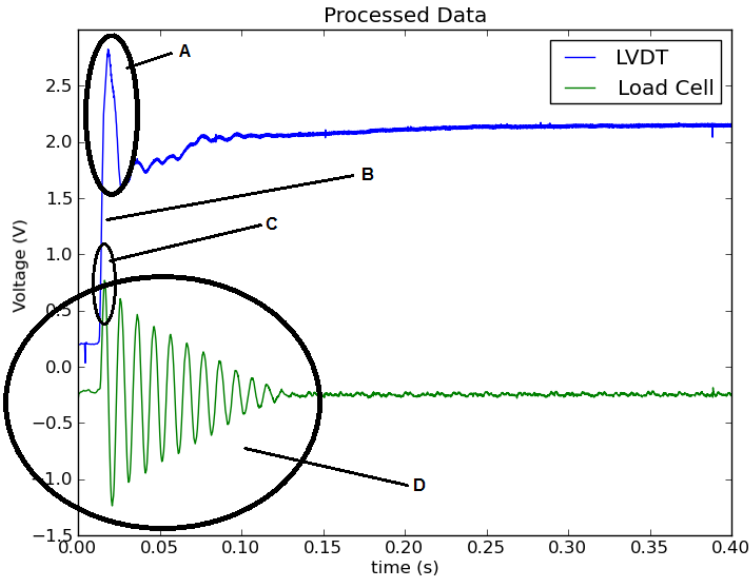

Figure 28: Processed Signals

When our signals were analyzed on the basis of velocity vs. time we noticed the trends seen in Figure 29. This figure shows that our transient period, where acceleration is occurring, is about 8mm for the case of 1000 RPM. This transient period is much greater than the period we required of approximately 1mm. A region of near-constant velocity was achieved. It would be preferable to engage and break the specimen in this region as the region is of sufficient length to break the sample.

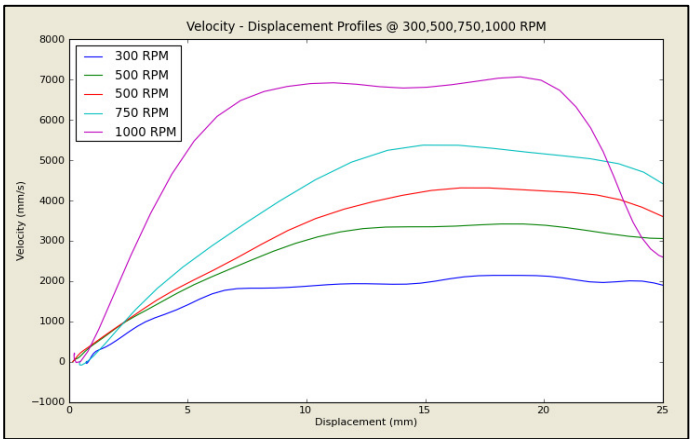

Figure 29: Velocity vs. Time Analysis

When analyzing both force and displacement simultaneously we expected to see the results of Figure 30. Our bovine pericardium samples are hybrid tissues with light strain characteristics dominated by elastin and high-strain characteristics dominated by collagen.

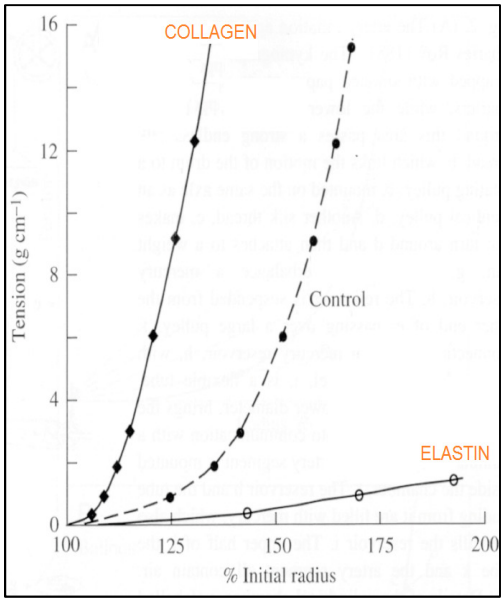

Figure 30: Documented Force vs. Displacement Characteristic for Sample

We were able to replicate this force-displacement curve using our device. The trends we witnessed are presented in Figure 31. We also were able to see a strain dependence of the resisting force. This data would not be of large significance to BME researchers because the data was collected during the acceleration phase of our device and we did not achieve the targeted $300s^{-1}$ rate when breaking the sample.

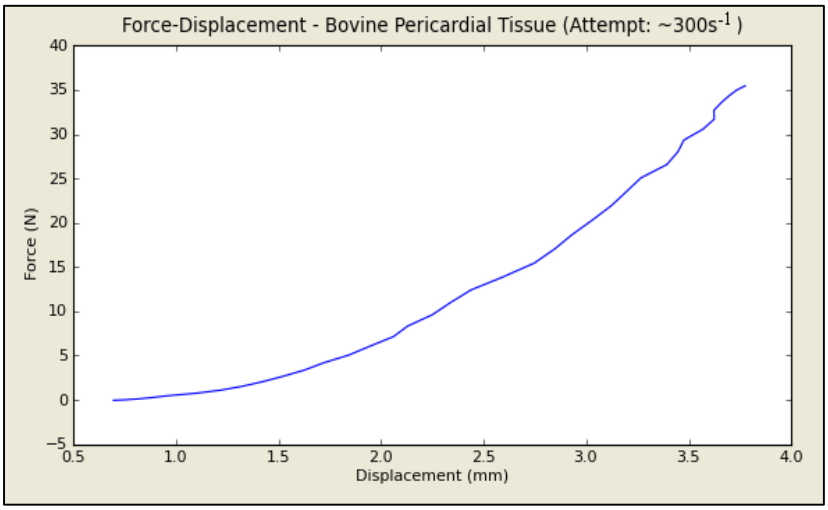

Figure 31: Force-Displacement Characteristic Obtained

10.4 *High Speed Video Testing Results*

In order to calculate the strain rate achieved during testing the approach was taken to use a high speed video camera and analyze the video using Photron Motion Tools software. Several videos were taken and analyzed; however, the one below was taken at 500 frames per second and a flywheel speed of 500RPM.

The selected software allowed the user to input a distance frame of reference, which then converted the distance to pixels per unit. Shown in Figure 32, is the user putting the distance of a bolt head of five millimeters, then software then converted the scale to 6.4 pixels per millimeter.

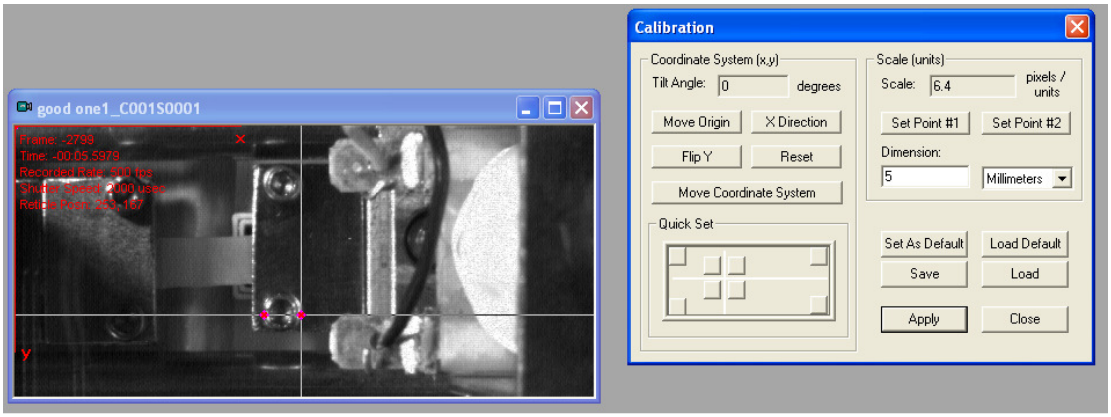

Figure 32: Creating a reference system for high-speed video analysis.

In the next step the user picks a location on the moving part and tracks it though several frames of video. The four frames below illustrate this process. In frame [1] a point on the moving part to be tracked is selected and tracked in subsequent frames (shown by red and green tracking dots). All of the frames are time stamped which allows for accurate data analysis.

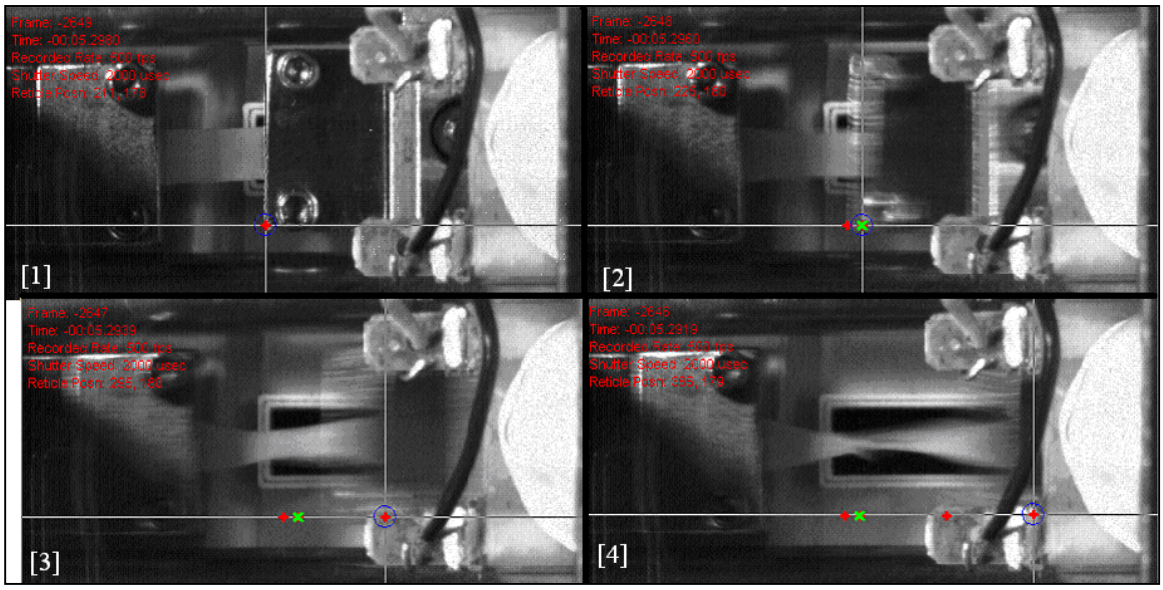

Figure 33: High-speed video frames and feature tracking for 8mm sample at 500RPM and 500 frames per second.

After the points have been selected the data is output to Excel for analysis. The data acquired from this trial is shown in

Table 5.

Table 5: Displacement data for 500RPM trial with 8mm sample

Frame	Time (seconds)	Track Point 1 (mm)

		x	y
-2649	-5.2980003	33.125	28.125
-2648	-5.2960005	35.15625	28.125
-2647	-5.2940001	46.09375	28.125
-2646	-5.2920003	57.1875	27.96875

From the output data, the velocity was found by dividing the distance by the time. In this case the maximum velocity was found by analyzing frames 2646 and 2647.

$$v = \frac{\Delta d}{\Delta t}$$

$$v = \frac{57.1875 - 46.09375}{-5.2920003 + 5.2940001}$$

$$v = 5547\ mm/s$$

From the calculated velocity and know the sample gauge length (8mm in this case) the strain rate can be found using the following formula:

$$\dot{\epsilon} = \frac{v}{l_0} = \frac{5547}{8} = 693.375\ \text{s}^{-1}$$

The maximum strain rate found for the device was calculated to be 814 s^{-1}; this was calculated using the same method as above at 1000RPM and an 8mm sample. The data acquired is outlined below in Table 6. Furthermore, it should be noted that the velocity below was in fact very similar to the LVDT velocity acquired for testing the device at 1000RPM; however, it was less than the predicted 10m/s during the design phase.

Table 6: Displacement data for 1000RPM trial with 8mm sample

Frame	Time	Track Point 1	
		x	y
-7218	-7.218000412	15.3488369	22.5581398
-7217	-7.217000484	17.4418602	22.5581398
-7216	-7.21600008	21.9767437	22.5581398
-7215	-7.215000153	28.4883728	22.6744194

For this set of data the team looked at frames 7215 and 7216.

$$v = \frac{\Delta d}{\Delta t}$$

$$v = \frac{28.4883728 - 21.9767437)}{-7.215000153 + 7.21600008}$$

$$v = 6512\ mm/s$$

$$\dot{\epsilon} = \frac{v}{l_0} = \frac{6512}{8} = 814\ \mathrm{s}^{-1}$$

It fell short of our design requirement of 1000s^{-1} however; we are quite satisfied with the result. Some of the items that held the team back in achieving the design requirement, included plastic yielding of the engagement pin at 1000RPM, and as a result the team could only effectively test the device up 700RPM on a regular basis. Furthermore, the device did not show the expected behavior and higher speeds did not always yield the best results. Additionally, the team did not see the acceleration that was expected (partially due to plastic yielding of the pin) and thus strain rates were not as high as 1000 s^{-1} as the sample was breaking during the acceleration and not at the maximum velocity.

10.5 *Time of Impact Analysis*

The bending force on the pin can be used to determine the interval of contact. The following calculations illustrate this phenomenon.

$$Sy = 205 \times 10^6 Pa$$
$$\sigma = \frac{My}{I}$$
$$M = Fd$$
$$F = \frac{\sigma I}{dy} = \frac{(205 \times 10^6 Pa)\left(\frac{\pi(0.00692m)^4}{64}\right)}{0.016m(0.00346m)} = 508.32\ N$$
$$m = housing, pin, grip, lvdt\ core + \frac{1}{3}\ (mass\ of\ beam\ and\ grips)$$
$$m = 239g + \frac{1}{3}\ (13.206g) = 243.4g$$
$$a = \frac{F}{m} = \frac{508.32N}{0.243kg} = 2088.4m/s^2$$
$$a = \frac{F}{m} = \frac{508.32N}{0.243kg} = 2088.4m/s^2$$
$$t = \frac{v}{a} = \frac{6m/s}{2088.4m/s^2} = 2.873 \times 10^3 s \cong 3ms$$

Our design requirements stated an incidence time of 1ms. However were not able to theoretically derive the time interval without knowing the forces that would be encountered.

11 Issues Encountered

This section outlines some of the issues that were encountered in testing and construction.

11.1 *Electrical and Mechanical Crosstalk*

Some of the unexpected results obtain from our data capture may have been a result of crosstalk.

Crosstalk was likely present in the propagation and coupling to the field, and between wires in our electronic system. The most common form of this crosstalk between electrical lines is where a transmission line shares a common path with another line (Christopoulos, 2007). In this case, current flow on one line results in an interference signal on the other line. Radiated interference is another coupling path. This interference does not involve a physical connection between the circuits

Another form of crosstalk we may have observed is that of mechanical cross-coupling depicted in Figure 34. The moving components (the housing, pin, and gripper) (shown as m_2) are coupled by the tissue (k_2, c_1) to the force transducer and grip (k_1, m_1). This was problematic for us as our measurement equipment was connected to the two cross coupled systems.

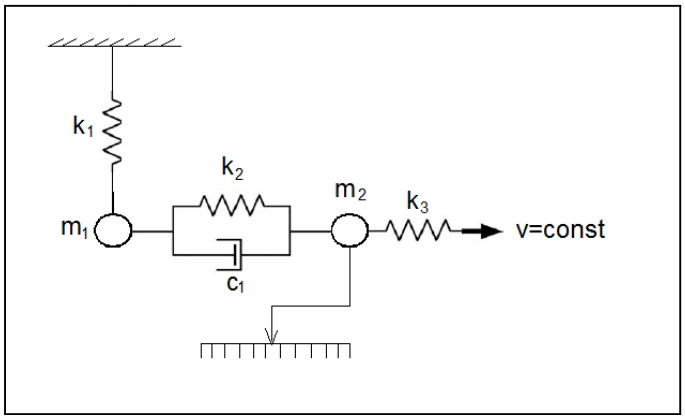

Figure 34: Mechanical Cross-Coupling

12 Impact on Society

In creating an effective and reliable device we hope to give Dr. Michael Lee a research tool that will help progress the state of biomaterials research. Thus, with this research

tool, valuable information will be obtained in how biomaterials fail in high impact (high strain rate) settings. With this information, Doctors could possibly learn how to better treat patients that have suffered impact injuries.

13 Life Cycle Analysis

The specimen's linear displacement and velocity will be fully determined when testing begins. At this point, the team will complete the design of the data acquisition system, specifically, regarding the LVDT measurement device and software.

14 Work Allotment

All fabrication was completed by in the Mechanical Engineering Machine Shop. The design entails cutting and machining. Table 7 compares the estimated time of machining to the actual amount of machining time required.

Table 7: Comparative Chart of Estimated to Actual Machining Hours

Part Description	Quantity	Estimated Hours	Quantity	Actual Hours
Flywheel	1	20	1	18
Flywheel pin	3	8	1	3
Grip top	2	6	2	5
Grip bottom	2	6	2	5
Tooth housing	1	10	1	11
Contact tooth	2	5	10	10
Frame	1	10	1	10
Plexiglas	1	5	1	4
Tooth holder	0	0	1	7
LVDT support	0	0	1	3
Force Transducer	0	0	1	4
Total Hours of Machining		**70 hrs**		**80 hrs**

The estimation of hours was low because some of the material for the parts was changed. The parts that were changed from carbon steel to stainless steel were more difficult to machine. The Mechanical Engineering Technicians completed the machining and the team completed the assembly, painting and electronics.

15 Budget

The estimated and final budget is illustrated in Table 4 and a detailed budget is located in Appendix D.

Table 8: Comparative Graph of Estimated to Actual Budget

Mechanical	Estimated	Actual

Frame	$150	$105
Flywheel	$40	$40
Specimen grip	$315	$172
Shock Absorber	$0	$67
Bearings	$0	$30
Main shaft	$65	$0
Electrical		
Motor	$335	$335
Measurement	$1000	$660
Tooth Engagement	$16	$16
Control	$330	$335
Power	$30	$0
Function Generator	$0	$375
Safety		
Polycarbonate	$0	$130
Modeling		
Rapid Prototyping	$0	$234
Misc		
	$1220	$50
Total		
	$3500	$2549

The project was funded both by the Department of Mechanical Engineering and the Department of Biomedical Engineering.

16 Future Considerations

This section outlines some refinements to the device that could be made in the future.

16.1 *Control of Initial Sample Length.*

The client has expressed that the ability to load samples into the apparatus to a predetermined length is desirable. At this point the operator loads the sample, tensions it, and then confirms the length. The current method of tensioning the sample is by moving the mounting block along the line of the arrow shown in Figure 35.

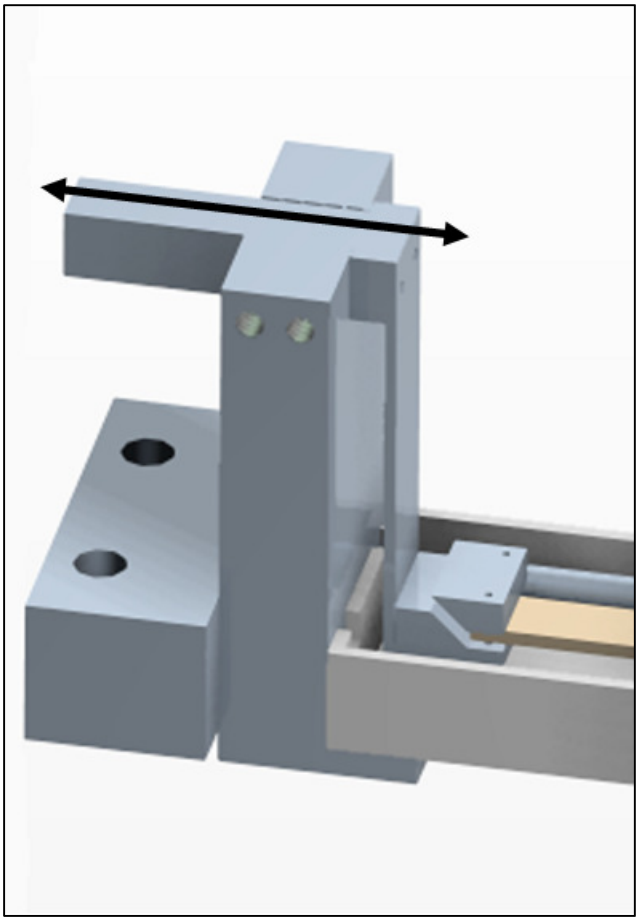

Figure 35: Current control of sample length

In the future, a calibrated drive screw mechanism could be implemented to move the mounting block with precision. This design would be similar to what is found on a precision microscopy stage.

16.2 *Prevent deformation of critical components*

In an effort to reduce deformation of the tooth component, the mass of the moving parts could potentially be reduced. This could be done by reducing mass by part redesign. Furthermore, material could be removed by drilling holes in non-critical areas of the moving parts. Other suggestions included changing material to aluminum or titanium. However, other issues arise with aluminum such as corrosion (due to the saline solution), and low yield strength. As well, titanium is substantially more expensive than steel, and more difficult to machine.

One example of reducing mass by component re-design would be to move the location of the spring acting on the pin. The current design shown in Figure 37 incorporates the spring below the tooth. Mass could be removed by placing the spring above the tooth holder.

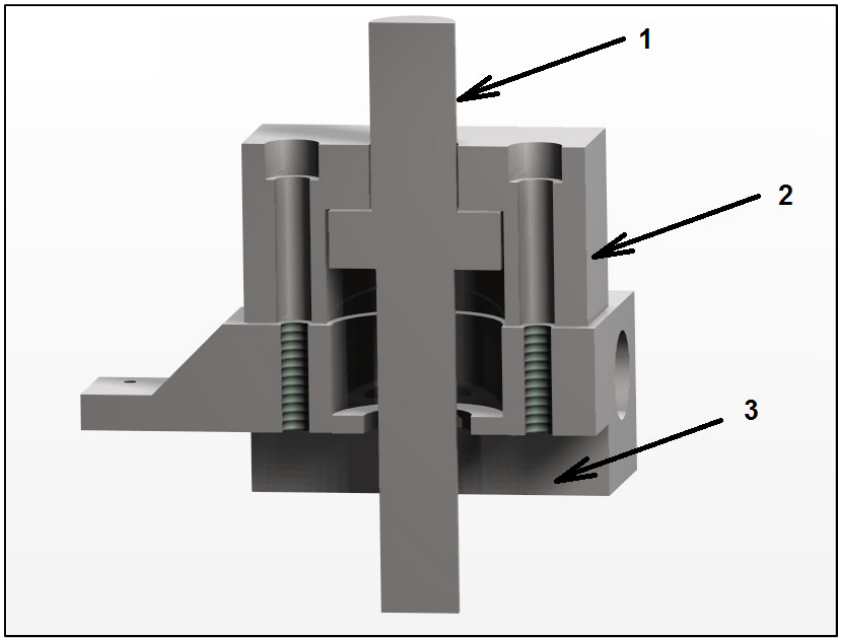

Figure 36: Cross-sectional view of spring loaded tooth.

Contact Tooth [1], Tooth holder [2], Tooth housing [3]

16.3 *Other Considerations*

The pin could be hardened to withstand tests with the motor run at 1000rpm. The shaft could be stepped to reduce ware when assembling/disassembling. In the future, a stainless steel bath could replace the current plastic one. This would allow the client to steam sterilize it between uses. The moment acting on the tooth could be reduced by minimizing the vertical distance between the bath, and the outer rim of the flywheel. This could be achieved by shimming the bearings, and motor mounts. Also, in an effort to reduce electrical crosstalk, dedicated circuit boards could be created, and shielded.

17 Conclusions

In conclusion the device constructed is able to achieve a strain rates of 800s-1 for samples of a typical length. This figure is 200s-1 short of our intended goal of 1000s-1. In addition a greater than anticipated transient period of acceleration was encountered indicating that minor machine modification would be necessary before the device is capable of research-quality work.

Despite these shortfalls many successes were encountered.

18 References

Cheng, M., Chen, W. Weerasooriya, T. “Mechanical Behavior of Bovine Tendon with Stress-Softening and Loading rate Effects.” Advanced Theory of Applied Mechanics V2, n2, 59-74. (2009)

Chen, W., Lu, F., Zhou, B. “A Quartz-crystal embedded Split Hopkinson Pressure Bar for Soft Materials.” Experimental Mechanics. V40, n1, 1-6 (March 2000)

Willett, T., Labow, R., Avery, N., Lee, M. “Increased Proteolysis of Collagen in an In Vitro Tensile Overload Tendon Model.” Annals of Biomedical Engineering.V35, n11, 1961-1972. (2007)

Active Power. Understanding Flywheel Energy Storage: Does high speed really imply a better design? White paper 112. <www.activepower.com>

Callister, W. Materials Science and Engineering, An Introduction, Edition Seven. John Wiley and Sons, Inc. (2007)

Lee. M. (2010) MECH 4650 Course Notes.

19 Appendices

List of Appendices

Appendix A – Previously Signed Documents
Appendix B –Decision-Making Tables and Charts
Appendix C –Gantt Chart
Appendix D –Budget
Appendix E –User's Manual
Appendix F –Engineering Drawings

Appendix A– Previously Signed Documents

List of Documents

Project Agreement
Project Waiver
Memorandum

Design Project Agreement

This Agreement is made and entered into for a term beginning the ____day of September 2009, and ending the ____day of May 2009 between:

Ben Breen

Ruth Domaratzki

Geoff Beck

Rachael Schwartz

(hereinafter referred to as "Design Team")

And

Dr. Michael Lee

(hereinafter referred to as "Client")

The Design Team and Client hereby agree as follows:

1] Scope of work

The scope of work agreed upon within the memorandum.

2] Principal investigators

The Principal investigators of the design project shall be the Design Team as stated above. (Students at the Department of Mechanical Engineering, Dalhousie University)

3] Confidentiality and Publication

The project and corresponding presentations, reports and web pages will be in the public domain.

4] Ownership of Intellectual Property

The intellectual property will remain the shared property of the Client and Design Team. The fabricated device will be the property of the Client. The project presentation and reports (with the exception of some possible proprietary information) will be in the public domain.

Design Project Waiver

This Agreement is made and entered into for a term beginning the ____day of September 2009, and ending the ____day of May 2009 between:

Ben Breen

Ruth Domaratzki

Geoff Beck

Rachael Schwartz

(hereinafter referred to as "Design Team")

And

Dr. Michael Lee

(hereinafter referred to as "Client")

The Design Team and Client hereby agree as follows:

Indemnity

Each party shall indemnify and save harmless the other party against all costs, actions, suits, claims, losses, or damages for all matters arising out of this agreement and the performance of the project. The Client shall indemnify the Design Team against all costs, suits, or claims resulting from the use by client or licensees of and deliverables or intellectual property developed by the Design Team under this agreement.

Warranties

Dalhousie University and the Design Team shall not be liable for any direct, indirect, consequential, or other damages suffered by the Client or any others resulting from the project or the use of the research results and data from the project or any such invention or product.

Entire Agreement

This agreement constitutes the entire agreement between the parties with respect to the subject matter hereof and supersedes all prior agreement, whether written or oral.

Memorandum

To: Dr. Julio Militzer
CC: Dr. Michael Lee, Dr. Kujath
From: Group 12 – Ben Breen, Ruth Domaratzki, Geoff Beck, and Rachael Schwartz
Date: 03/10/09
Re: Design Requirements for Loading Apparatus for High Velocity Tissue Rupture (LAHVTR)

Summary of the Project

Our group will be designing a loading apparatus with the capability to conduct fractures of a controlled and rapid nature in collagen-rich tissues (bovine tendon) for Dr. Lee of the school of Biomedical Engineering. After meetings with Dr. Lee, the design requirements have been set, and are outlined below.

Design Requirements

The requirements have been set under the following categories:

Size: The device should be able to fit on a table top with one face approximately $30 \times 30\ cm$.
Strain Rate: The strain rate achievable should be on the order of 100
Loading: Achieve a minimum of $1/100$ loading
Lifetime: Should last approximately 5 yrs
Conditions: The conditions of the test sample will be as close as possible to physiological conditions (100% humidity at 37˚C)
Control: The device will be designed so the operator has control of the strain rate.
Safety Features: The device will be designed to be safely operated by trained individuals. A shielding component will be incorporated if required.
Documentation: The device will be accompanied with a comprehensive instruction manual.
Timing and Deadlines: All set deadlines and time requirements set out in the MECH 4010/4020 Design Project Handbook will be met.
Data Acquisition: The device should provide data describing the force, displacement, and time for each trial.

Intellectual Property

The intellectual property will remain the shared property of the Client and Design Team. The fabricated device will be the property of the Client. The project presentation and reports (with the exception of some possible proprietary information) will be in the public domain.

Provisions by Client

The client will provide:
Time-weekly meetings
Funding- Fabrication costs, supplies

Appendix B: Decision-Making Tables and Charts

Group 12: Brainstorming Session
Morphological Chart for High Velocity Loading Apparatus

Table 1: Components of the Design Compared

Component		Solutions				
1	Propulsion	Pendulum	HSBA	DC Actuator	Electromagnetic	Flywheel
2	Velocity measurements	LVDT	ADC + LPT1	Piezo-based	Oscilloscope	Laser
3	Force measurement	Laser	Load cell			

Table 2: Options Selected

Design	Propulsion	Velocity measurements	Force measurement
1	Pendulum	Laser	Laser
2	Pendulum	LVDT	Load cell
3	Hopkinson bar	Laser	Load cell
4	Flywheel	Laser	Load cell
5	Flywheel	LVDT	Load cell
6	Hopkinson bar	Laser	Laser
7	Flywheel	Laser	Laser
8	DC Actuator	Laser	Laser
9	Electromagnetic	Laser	Load cell

Table 3: Evaluation Criteria

	Complexity	Speed Performance	Accuracy in Speed	Controllability in Speed	Accuracy in Measurement	Cost Estimate	Total
1	9	7	9	6	7	7	45
2	10	7	9	6	8	9	49
3	2	6	9	8	10	7	42
4	9	10	10	9	9	10	57
5	6	9	9	9	7	7	47
6	5	10	9	9	10	5	48
7	8	10	10	9	9	1	47
8	8	4	4	4	6	7	33
9	4	6	7	7	8	3	35

Table 4: Tabulation of Votes

Design	Ruth	Rachael	Geoff	Ben	Total
6	3	1	2	3	9
2	2	3	3	2	10
4	1	2	1	1	5

House of Quality

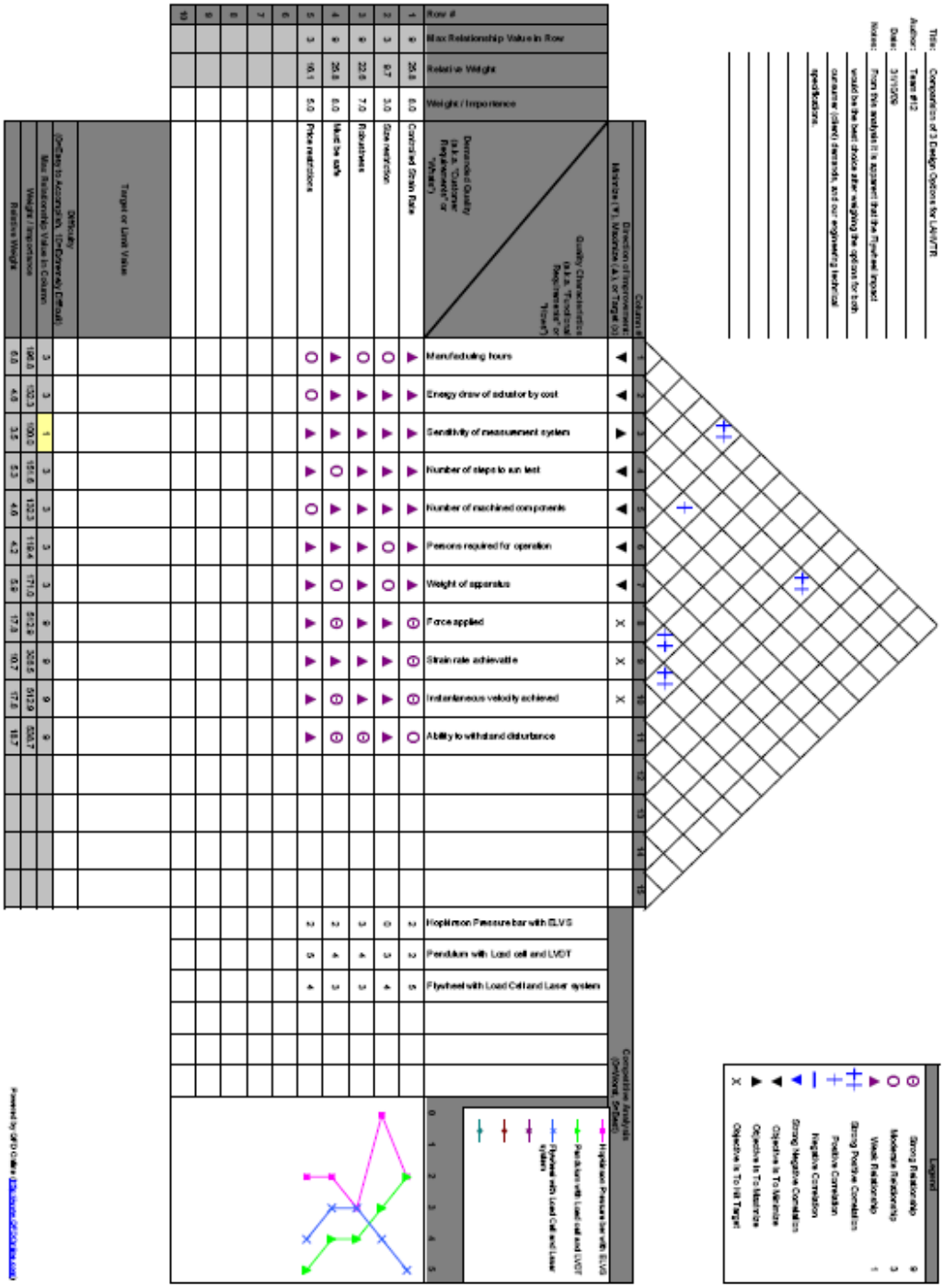

Appendix C: Gantt Chart

(see attached)

Appendix D: Budget

Item Description	Location in Design Hierarchy	Item Status	Distributer	Quantity	Total (No Tax)
0.06" Sheet Metal	Mech/Frame	Essential	Metals-R-Us (Dartmouth)	12	$74.88
Rapid Prototyping	Misc	Essential	Dalhousie		$233.72
Stainless Steel	Mech/Shaft	Essential	Metals-R-Us (Dartmouth)	1	$172.39
Shock Absorber	Mech/Frame	Essential	McMaster-Carr	1	$67.16
Flywheel	Mech/Shaft	Essential	Metals-R-Us (Dartmouth)	1	$40.00
1.25" Square Tube	Mech/Specimen Grip	Essential	Metals-R-Us (Dartmouth)	2	$35.56
External retaining rings	Mech/Specimen Grip	Essential	Mechanical Dept	4	$0.00
Shaft	Mech/Shaft	Essential	Mechanical Dept	1	$0.00
Plummer Block Bearings	Mech/Shaft	Essential	Fastenal	2	$30.00
LVDT	Elect/Measurement/Displacement	Essential	A-Tech	1	$401.00
Motor	Elect/Motor	Essential	Motion Industries (Dartmouth)	1	$226.78
Frequency controller	Elect/Motor	Essential	Motion Industries (Dartmouth)	1	$334.96
12VDC Pin Driving Solenoid	Elect/PinEngagement	Essential	McMaster-Carr		$15.27
Strain Gages	Elect/Measurement/Displacement	Essential	Intertechnology	10	$135.00
Precision Resistors	Elect/Measurement/Displacement	Essential	Intertechnology	4	$80.00
Titanium	Elect/Measurement/Displacement	Essential	Alfa Aesar	1	$43.70
Polycarbonate	Safety	Essential	Piedmont Plastics (Dartmouth)	1	$130.71
Function Generator	Elect/Control	Essential	Allied Electronics	2	$375.00
Miscellaneous	Misc	Essential		1	$50.00
				TOTAL	**$2,446.13**

Mechanical Department Budget

Item Description	Mechanical Department Funds	SELF Funds	Total
RP Prototyping	$106.86		$106.86
RP Prototyping	$55.80		$55.80
McMaster Carr		$131.84	$131.84
Metals R Us	$25.64	$110.24	$135.88
Metals R Us		$62.15	$62.15
Piedmont Plastics		$130.71	$130.71
RP Prototyping	$11.70		$11.70
Ben Breen		$40.47	$40.47
RP Prototyping		$15.72	$15.72
RP Prototyping		$2.34	$2.34
RP Prototyping		$15.66	$15.66
TOTAL	**$200.00**	**$509.13**	
	GRAND TOTAL	**$709.13**	

Appendix E: User's Manual

User Manual for Loading Apparatus for High Velocity Tissue Rupture

---

Team 12

Ben Breen

Geoff Beck

Rachael Schwartz

Ruth Domaratzki

This manual contains an overview of the safe operation of the Loading Apparatus for High Velocity Tissue Rupture (LAHVTR)

1. General Use

The apparatus is designed to perform tensile tests on biological tissues at strain rates at a strain rate of $1000s^{-1}$. The loading apparatus will fracture a specimen of bovine tendon (up to 2.5cm), recording force, position, and velocity.

2. Safety Precautions

The Loading Apparatus for High Speed Tissue Rupture holds several areas of safety concern. This section is to inform the operator of the risks and necessary precautions taken to operate the equipment.

The flywheel is rotating at high speeds. The following precautions should be taken when operation the device:

> Place the **safety shield** over the flywheel whenever before operating the motor. Refer to Figure 1 for the correct orientation of the safety shield.
>
> **Safety glasses** and **hearing protection** must be worn.
>
> **Remove loose clothing and jewelry** prior to operating the equipment.
>
> Before each test, **inspect the apparatus** to make sure that no tools or wires are in the vicinity of the flywheel.

Avoid contact with the shaft coupling. The coupling experiences high temperatures during and after operation.

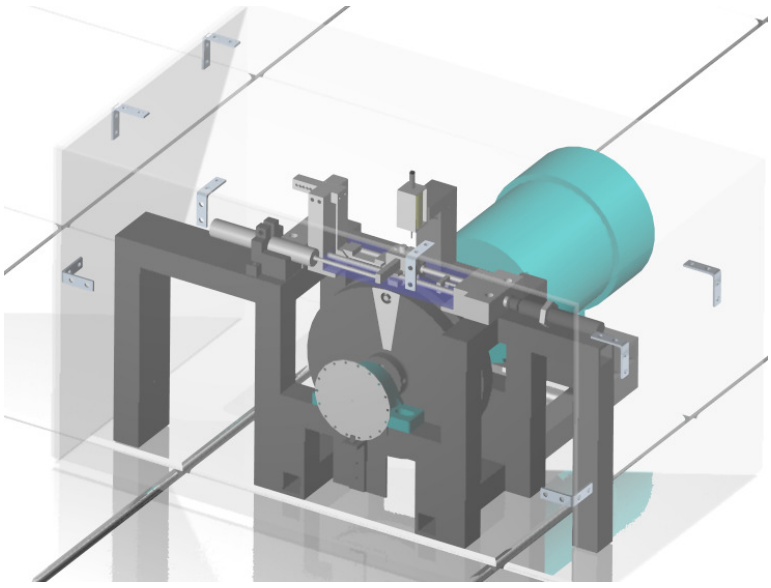

Figure 1: Correct Safety Shield Orientation

3. Initial Operation and start up checklist

Before operating the LAHVTR apparatus, read Section 2 of this manual carefully and adhere to all safety precautions. Before each test session, complete a visual inspection of the apparatus and complete the Start-up Checklist located in Appendix A.

4. Operating Instructions

4.1 The Strobotac

The Strobotac is used to determine the frequency of the rotation of the flywheel in operation. The Strobotac is placed on the tabletop at a distance of one foot from the face of the flywheel. Dimming the laboratory lights may aid in the ease of reading the frequency of the rotation of the flywheel. The RPM dial is used to select the RPM range in which the operator will test. The LAHVTR operates at a maximum of 1000 rotations per minute. For this reason, the operator will select in the operating range of 110-690 rpm or 670-4170 rpm. The outer surface of the RPM dial is the precision control. The dial is adjusted to the frequency of rotation at which the testing is performed. Turn on the Strobotac, the frequency controller, and the power supply. Adjust the frequency control (using the arrow keys) until the white stripe painted on the flywheel seems to slow and stop. At this point, the frequency of the stroboscope equals the frequency of rotation of the flywheel. The frequency controller displays the frequency of the rotation of the flywheel in rotations per minute while the shaft is rotating.

4.2 Sample Loading

Loosen the screws on the clamps and remove the tops of the clamps (Figure 1, [4]). Place these parts on the laboratory table. The sample should be precisely measured and not exceed the length of one centimeter. Attach the sample to clamps by placing the sample on the clamp bottoms (Figure 2, [3]) and tightening the screws with supplied the Allen key. Loosen the setscrews (Figure 2, [1]) and apply tension to the sample by adjusting the outcropping of the load cell. Tighten the setscrews using the supplied Allen key.

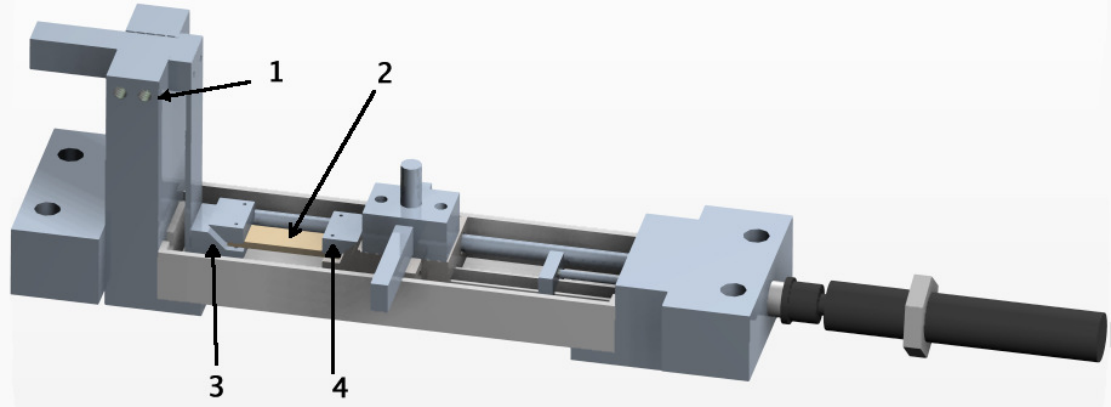

Figure 2: Linear Track - Setscrews [1], Biological sample [2], Grip bottom [3], Grip top [4]

4.3 Power source

The power supply can be used as a current source. The set-up of this method is described below.

1. Connect the desired circuit to the power supply output terminals.

2. Turn the power supply on. The power supply's outputs will be disabled (the OFF annunciator is on).

3. Enable the outputs by pressing the Output On/OFF key (see Point 8, Figure 3) The CV and +6V annunciators will be on to indicate that the power supply operates in the *constant voltage* mode and that the +6V display is selected. The display is in the *meter* mode, i.e. the display shows the actual output voltage and current. To set up the +25 V power supply, press the **+25V** key to select the display and adjust the +25V supply voltage. Do the same for the -25V supply.

4. Set the display for *limit* mode by pressing the Display Limit key (see Point 3, Figure 3). You will notice the LMT annunciator blinking to indicate that the display is in the *limit* mode. The display shows the actual voltage and current limit values of the selected supply.

5. You will notice that the second digit of the voltmeter is blinking. Turn the large knob to set the desired voltage *limit* (make sure the LMT annunciator is still blinking).

6. Press the Vol/Cur key (see Point 11, Figure 3). The second digit of the ammeter will be blinking. Adjust the desired output current that the current source will supply.

7. To return to the *meter* mode press the Display Limit (see Point 3, Figure 3) or let the display time-out to return automatically to the *meter* mode. The LMT annunciator will be off[3].

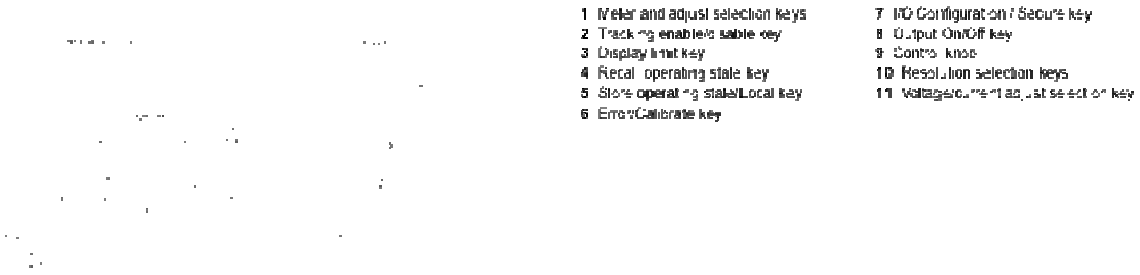

Figure 3- Front panel of the E3631A power supply[4]

[3] University of Pennsylvania, Department of Electrical Engineering. "Basics of Power Supplies -Use of the HP E3631A Programmable Power Supply." Web Mar 27, 2010. http://www.ese.upenn.edu/rca/instruments/HPpower/PS3631A.

4.4 Flywheel Operation

Turn the power to the frequency controller on. Gradually increase the speed of the motor by pressing the upward arrow key until desired test speed is reached. When the test is complete, gradually slow the flywheel by pressing the downward arrow key. Turn off the power to the frequency controller.

5. Maintenance

Preventative maintenance should be performed on the LAHVTR to reduce risk of failure.

Before performing testing on the LAHVTR, inspect the contact pin for chipping or deformation. Replace the pin if needed.

Dismantle and clean all parts of the LAHVTR exposed to biological tissue. Use warm water and a disinfecting soap.

[4] Agilent Technologies (2000). User's Guide - Agilent E3631A Triple Output DC Power Supply.

Appendix A

Start-up Checklist					
Issued by:		Effective date:			
Report No:		Inspector:			
Full Speed Motor Test:		**Action Taken:**		**Replacement:**	
	1. Sound form bearings		1. Adjustment		1. Complete
	2. Balance - vibration present		2. Replacement		2. Partial
	3. Flywheel electric components		3. Repaired		3. None
	4. Other		4. Other		
Maintenance Action Required as a Result of:					
	1. Suspected Failure or Malfunction				
	2. Improper Maintenance				
	3. Damaged Accidently				
Symptoms:		**Visual Inspection:**		**Cause of Trouble:**	
	1. Inoperative		1. Threads worn		1. Design Deficiency
	2. Interference		2. Tarnish		2. Faulty Maintenance
	3. Difficult to use		3. Chipped/cracked contact pin		3. Faulty Sterilization
			4. Spring tension		4. Foreign Object
			5. Sharp edges		5. User Adjustment
			6. Exposed wiring		6. Wrong Part Used
			7. Loose components		7. Undetermined
					8. Other
Disposition or Corrective Action:					
I. Reason for No Action:		**II. Action:**		**III. Follow up**	
	1. Lack of Facilities		1. Pull from Operation		1. Scheduled
	2. Lack of Personnel		2. Adjusted		2. Performed
	3. Lack of Repair Parts		3. Repaired		
	4. Other		4. Retest and Hold		
			5. Other		

Maintainability Information:	Hours	Min	Team Member:
Time to Locate Trouble			
Time to Repair/Replace			
Total Time Non-Operative			

Remarks (Furnish additional information concerning failure of corrective action)

Department:	Signature:	Date:

Appendix F: Engineering Drawings

List of Drawings
(See Attached)

Frame Explosion L-00-00

Frame Explosion L-01-00

1. Bottom Mount L-01-01
2. Horizontal Mount L-01-02
3. Grip Support L-01-03
4. Removable Block L-01-04
5. LVDT Support L-01-05
6. Removable Block [2] L-01-06
7. Vertical Mount L-01-07
8. Bearing Mount L-01-08
9. Bearing Mounts L-01-09

Test Bed Explosion L-02-00

1. Linear Track Block B L-02-01 – Drawing 1
2. Linear Track Block B L-02-01 – Drawing 2
3. Linear Track Block L-02-02
4. Specimen Bath L-02-03 – Drawing 1
5. Specimen Bath L-02-03 – Drawing 2
6. Specimen Grip 2 L-02-04
7. Grip Top L-02-05
8. Tooth Guide L-02-06 – Drawing 1
9. Tooth Guide L-02-06 – Drawing 2
10. Impact Tooth L-02-07
11. Bushing L-02-08
12. Damper Plate L-02-09
13. Damper Rod L-02-10
14. Stain Block L-02-11
15. Guide Shaft L-02-12
16. Housing Stop Plate L-02-13
17. Load Cell L-02-14
18. Tooth Housing L-02-15 – Drawing 1
19. Tooth Housing L-02-15 – Drawing 2
20. Tooth Housing L-02-15 – Drawing 3

Flywheel Explosion L-03-00

1. Flywheel L-03-01 – Drawing 1
2. Flywheel L-03-01 – Drawing 2
3. Flywheel L-03-01 – Drawing 3
4. Engagement Pin L-03-02
5. Main Shaft L-03-03